



Frontiers paper

Origin of a global carbonate layer deposited in the aftermath of the Cretaceous-Paleogene boundary impact



Timothy J. Bralower ^{a,*}, Julie Cosmidis ^b, Peter J. Heaney ^a, Lee R. Kump ^a, Joanna V. Morgan ^c, Dustin T. Harper ^d, Shelby L. Lyons ^a, Katherine H. Freeman ^a, Kliti Grice ^e, Jens E. Wendler ^f, James C. Zachos ^g, Natalia Artemieva ^h, Si Athena Chen ^a, Sean P.S. Gulick ⁱ, Christopher H. House ^a, Heather L. Jones ^a, Christopher M. Lowery ^j, Christine Nims ^a, Bettina Schaefer ^e, Ellen Thomas ^{k,l}, Vivi Vajda ^m

^a Department of Geosciences, Pennsylvania State University, University Park, PA, 16802, USA^b Department of Geosciences and Earth and Environmental Systems Institute, Pennsylvania State University, University Park, PA, 16802, USA^c Department of Earth Science and Engineering, Imperial College London, UK^d Department of Geology, The University of Kansas, Lawrence, KS 66045, USA^e WA-Organic and Isotope Geochemistry Centre, The Institute for Geoscience Research, School of Earth and Planetary Science, Curtin University, Perth, WA, Australia^f Institute of Geosciences, Friedrich-Schiller-University Jena, Burgweg 11, 07749 Jena, Germany^g Earth and Planetary Sciences, University of California Santa Cruz, 1156 High Street, Santa Cruz, CA 95064, USA^h Planetary Science Institute, Tucson, AZ, USAⁱ Institute for Geophysics and Dept. of Geological Sciences, Jackson School of Geosciences, & Center for Planetary Systems Habitability, University of Texas at Austin, USA^j Institute for Geophysics, Jackson School of Geosciences, University of Texas at Austin, USA^k Department of Geology and Geophysics, Yale University, New Haven CT 06520, USA^l Department of Earth & Environmental Sciences, Wesleyan University, Middletown CT 06459, USA^m Department of Palaeobiology, Swedish Museum of Natural History, Stockholm, Sweden

ARTICLE INFO

Article history:

Received 19 February 2020

Received in revised form 21 June 2020

Accepted 10 July 2020

Available online xxxx

Editor: L. Derry

Dataset link: <https://www.pangaea.de/>

Keywords:

K-Pg boundary

micrite

cyanobacterial bloom

Chicxulub

ABSTRACT

Microcrystalline calcite (*micrite*) dominates the sedimentary record of the aftermath of the Cretaceous-Paleogene (K-Pg) impact at 31 sites globally, with records ranging from the deep ocean to the Chicxulub impact crater, over intervals ranging from a few centimeters to more than seventeen meters. This micrite-rich layer provides important information about the chemistry and biology of the oceans after the impact. Detailed high-resolution scanning electron microscopy demonstrates that the layer contains abundant calcite crystals in the micron size range with a variety of forms. Crystals are often constructed of delicate, oriented agglomerates of sub-micrometer mesocrystals indicative of rapid precipitation. We compare the form of crystals with natural and experimental calcite to shed light on their origin. Close to the crater, a significant part of the micrite may derive from the initial backreaction of CaO vaporized during impact. In more distal sites, simple interlocking rhombohedral crystals resemble calcite precipitated from solution. Globally, we found unique calcite crystals associated with fossilized extracellular materials that strikingly resemble calcite precipitated by various types of bacteria in natural and laboratory settings. The micrite-rich layer contains abundant bacterial and eukaryotic algal biomarkers and most likely represents global microbial blooms initiated within millennia of the K-Pg mass extinction. Cyanobacteria and non-haptophyte microalgae likely proliferated as dominant primary producers in cold immediate post-impact environments. As surface-water saturation state rose over the following millennia due to the loss of eukaryotic carbonate producers and continuing river input of alkalinity, “whittings” induced by cyanobacteria replaced calcareous nannoplankton as major carbonate producers. We postulate that the blooms grew in supersaturated surface waters as evidenced by crystals that resemble calcite precipitates from solution. The microbial biomass may have served as a food source enabling survival of a portion of

* Corresponding author.

E-mail addresses: bralower@psu.edu (T.J. Bralower), jxc1158@psu.edu (J. Cosmidis), pjh14@psu.edu (P.J. Heaney), lrk4@psu.edu (L.R. Kump), j.v.morgan@imperial.ac.uk (J.V. Morgan), dtharper@ku.edu (D.T. Harper), slyons@psu.edu (S.L. Lyons), khf4@psu.edu (K.H. Freeman), KGrice@curtin.edu.au (K. Grice), wendler@uni-bremen.de (J.E. Wendler), jzachos@ucsc.edu (J.C. Zachos), artemeva@psi.edu (N. Artemieva), chensi951222@gmail.com (S.A. Chen), sean@ig.utexas.edu (S.P.S. Gulick), c.h.house@gmail.com (C.H. House), heatherjones394@gmail.com (H.L. Jones), cmlowery@utexas.edu (C.M. Lowery), cwn7@psu.edu (C. Nims), bettina.schaefer@postgrad.curtin.edu.au (B. Schaefer), ellen.thomas@yale.edu (E. Thomas), Vivi.Vajda@nrm.se (V. Vajda).

the marine biota, ultimately including life on the deep seafloor. Although the dominance of cyanobacterial and algal photosynthesis would have weakened the biological pump, it still would have removed sufficient nutrients from surface waters thus conditioning the ocean for the recovery of biota at higher trophic levels.

© 2020 Elsevier B.V. All rights reserved.

1. Introduction

The mass extinction at the Cretaceous-Paleogene (K-Pg) boundary (66.0 Ma) eliminated ~75% of marine and ~50% of terrestrial species (Sepkoski, 1996). In the ocean, the extinction was highly selective with near-surface organisms more susceptible to extinction than deep-water dwellers (e.g., Jablonski, 1986), and calcifying organisms more susceptible than those with siliceous or organic tests (e.g., Thierstein, 1982). The resulting disruption of food webs paved the way for rapid diversification of new life in the Paleocene oceans (e.g., Alroy, 2008; Hull et al., 2011).

The dominant group of Cretaceous phytoplankton, the calcareous nannoplankton, suffered extinction of 88% of genera and 93% of species at the K-Pg boundary (Bown et al., 2004). The extinction was abrupt and striking (e.g., Bown, 2005) and a diverse group of some 131 species, many of which had been successful for millions of years, were replaced within a few thousand years by a handful of taxa including a series of ephemeral but dominant species, the so-called “boom-bust” taxa (Jones et al., 2019). The sharp taxonomic turnover involved a radical change in the degree of calcification and cell size from more heavily-calcified and larger-celled Cretaceous species to the less heavily calcified “boom-bust” taxa with smaller cell sizes (Alvarez et al., 2019). Among the phytoplankton, nannoplankton never regained their dominance and were replaced by diatoms and dinoflagellates, especially in eutrophic, high latitude and coastal settings (Katz et al., 2004; Knoll and Follows, 2016). Biogeochemical cycles were radically transformed at the K-Pg boundary as a result of these evolutionary shifts, involving change in carbonate saturation and accumulation rates, and organic carbon export and burial (e.g., Zachos and Arthur, 1986; Kump, 1991; D'Hondt, 2005; Henehan et al., 2016; Alvarez et al., 2019; Sepulveda et al., 2019). However, questions remain about the rate and magnitude of these changes, and exactly how they relate to the biotic recovery in the surface and deep ocean. Model simulations suggest that the extinction of calcareous nannoplankton would lead to an increase in saturation over thousands of years in a so-called saturation “overshoot”, possibly resulting in a brief interval of supersaturation (Alegret and Thomas, 2013; Henehan et al., 2016). Recent B isotope measurements support these simulations showing a brief interval of increased saturation following a short interval of acidification (Henehan et al., 2019). Moreover, sediments in lowermost Paleocene sections from numerous sites are rich in microcrystalline calcite, known as micrite (Thierstein et al., 1991; Bralower et al., 2002; Minoletti et al., 2005), which has been proposed to result from abiotic calcite precipitation (Bralower et al., 2002). However, the extent of micritic sediments is not known and cause of deposition is not fully established.

Numerous independent lines of evidence support the impact at Chicxulub as the main trigger of the mass extinction and related changes in biogeochemical cycles (Hildebrand et al., 1991; Schulte et al., 2010; Hull et al., 2020). These changes occurred so rapidly that they are recorded in a few centimeters of section at most localities worldwide (D'Hondt et al., 1994; Kring, 2007), typically making it difficult to reconstruct events shortly after the impact. Coring of the peak ring of the Chicxulub crater [International Ocean Discovery Program (IODP) and International Continental Drilling Program (ICDP) Expedition 364, Site M0077] recovered a highly expanded record of the immediate aftermath of the im-

pact (Morgan et al., 2016), allowing exploration of the earliest recovery in unprecedented detail. The section at Site M0077 includes 130 m of impact melt rock and melt-bearing impact breccia (“suevite”). Most suevite was deposited in a flooded crater following ocean resurge, and the shallowest suevite record tsunami (Gulick et al., 2019). The ‘transitional unit’, a 75 cm interval of micritic limestone directly overlying the suevite, consists of sediment that settled from turbid waters, and recorded the return of life to the sterilized crater in the days and years after the impact, along with changes in ocean chemistry (Lowery et al., 2018; Schaefer et al., 2020).

Here, we report the discovery that the micrite-rich layer found in the crater is actually a global feature of the K-Pg boundary aftermath, based on observations at 30 other sites across the world's oceans, and show that it contains fragile crystals with an array of morphologies. Based on comparison with the morphology of natural and experimental materials, we propose that the micrite has several origins including precipitation from supersaturated seawater, initially via carbonation of impact-generated CaO and later by a survivor microbial community thriving in the millennia after of the mass extinction. We propose that long term supersaturation was caused by a sharply lowered CaCO_3 /organic carbon rain ratio resulting from the pelagic calcifier extinction, and continued river alkalinity delivery that gradually led to surface seawater calcite saturation states sufficient to allow “whitings”, consistent with model results (Henehan et al., 2016). We postulate that this microbial community was uniquely adapted to thrive under the effects of the Chicxulub impact, provided food for survivors at higher levels in the food chain in its aftermath, and helped condition ocean environments for the recovery of decimated groups. In the crater, the microbial community was part of a diverse group of primitive life adapted to post-impact environmental upheaval (Schaefer et al., 2020).

2. Materials and methods

Materials: This study is based on observations of a total of 818 bulk sediment samples from 31 sites where the K-Pg boundary is preserved, ranging from proximal locations in the Gulf of Mexico (including within the Chicxulub crater), through a range of shelf to abyssal depths in all ocean basins (Fig. 1; Table 1). K-Pg boundary units were deposited via ejecta, high-energy tsunami and seiche waves, and gravity flows at proximal Gulf of Mexico and crater sites and by pelagic sedimentation at sites in other ocean basins, and have highly variable lithology, CaCO_3 content, and color. Sections were studied at centimeter to decimeter resolution. More information on sites is provided in Supplemental Materials Section 3.

Light Microscopy: Smear slides were prepared of all bulk sediment samples using routine techniques and observed in a Zeiss Axio Imager A2 photomicroscope at a magnification of 1600x. Observations focused on micrite and nannofossils (including calcispheres). Fragments of foraminifera and occasional whole juvenile foraminifera were also observed.

Scanning Electron Microscopy: Micrite and associated particles were observed in a FEI Nova NanoSEM 630 Field-Emission SEM (FE-SEM) at the Materials Characterization Laboratory at Pennsylvania State

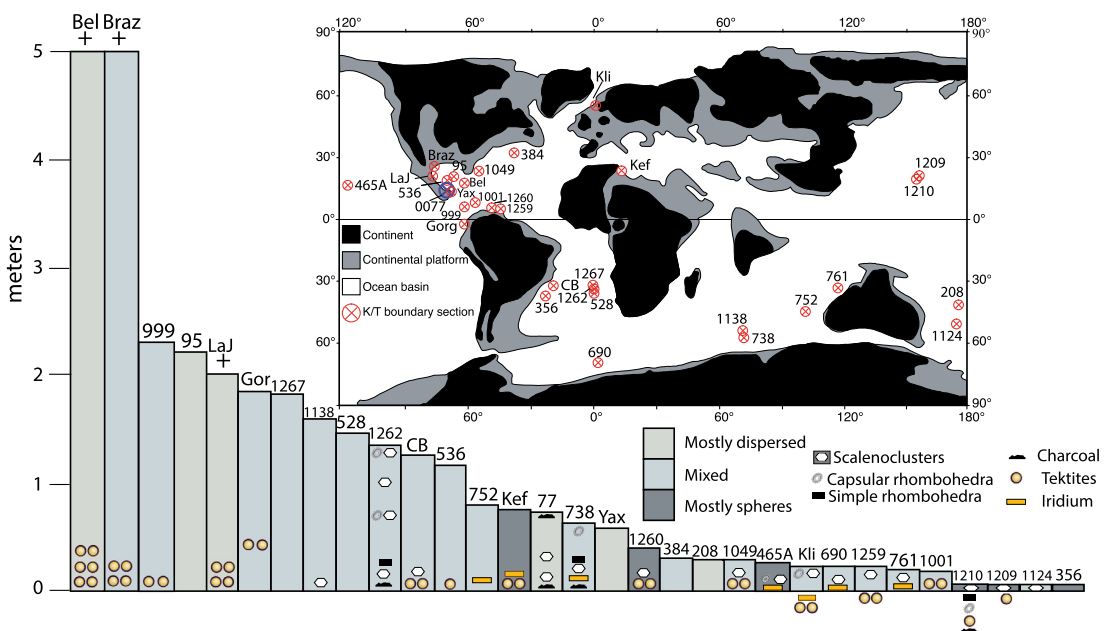


Fig. 1. Occurrences (red crosses) of the global micrite-rich layer at the K-Pg boundary. Blue circle indicates location of the Chicxulub impact crater. Columns show thickness of micrite-rich layer at 31 sites with interval over 5 m not shown (Bel, Braz). + indicates minimum thickness in sections where uppermost samples collected are still within layer. Colors of columns refer to nature of micrite: largely dispersed refers to intervals dominated by single micrite grains; spheres to intervals dominated by translucent spheres, shelled scalenohedra; and mixed to both. Occurrences of different micrite structures indicated by symbols, as are K-Pg boundary markers (Ir, charcoal and tektites). Symbols beneath condensed columns occur within the post boundary section (not below). Numbers refer to DSDP/ODP/IODP Sites. Bel-Beloc, Haiti; Braz-Brazos, Texas; LaJ-LaJilla, Mexico; Gor-Gorgonilla, Colombia; CB-Campos Basin, South Atlantic; Kef, El Kef, Tunisia; Yax, Yaxcopoil borehole, Chicxulub crater; Kli-Stevns Klint, Denmark.

University (PSU). To observe the fine fraction, bulk sediment samples were disaggregated in water. A few drops of the solution were placed on a corner of a coverslip and slowly dried on a hotplate. The piece of coverslip was adhered to an SEM stub using carbon tabs. Samples were coated with Ir and viewed in the SEM using immersion imaging mode, typically with a working distance about 3.2 mm, accelerating voltage of 7 kV and spot size of 2.8 nm. Energy Dispersive Spectroscopy was used to identify unknown particles based on their elemental composition. These analyses were performed routinely at first in all samples until a clear relationship between morphology and chemical composition was established. The sizes of particles were determined manually using ImageJ software.

Transmission Electron Microscopy: Ultrathin sections of Sample 738C-20R-5, 97 cm were prepared for TEM study using a standard microbiology protocol in order to preserve potential microbial or organic structures. The bulk sediment sample was fixed with glutaraldehyde and post-fixed with osmium tetroxide in HEPES buffer, then dehydrated with ethanol and propylene oxide and embedded in an Epoxy resin (Epoxy embedding medium kit, Sigma-Aldrich Co.). Ultrathin sections (~70 nm) were obtained using diamond knife ultramicrotomy. TEM analyses were performed using a Talos F200X at PSU equipped with a field emission gun and operating at 200 kV. Scanning transmission electron microscopy (STEM) observations were performed in the high angle annular dark field mode. Chemical maps were obtained using Energy Dispersive X-ray Spectroscopy (EDXS) with a Super-X system consisting of 4 SDDs (Silicon Drift Detectors). A sample from Site 1262 (1262B-22H-4, 134 cm) was disaggregated and dried on a copper grid for TEM study.

Observations of foraminifera: Foraminifera were generally rare in samples compared to the fine fraction. To observe foraminifera and other larger particles in the SEM, samples were centrifuged to remove clay, coccoliths, and fine micrite. The coarser fraction was placed on a double-sided carbon tab on the SEM stub using a pipette. Samples were also sieved to isolate the foraminiferal frac-

tion. To prepare samples for washing, they were broken down into pea-sized pieces, placed in a mixture of water and hydrogen peroxide on a shaker table overnight. Samples were washed through a 38 µm sieve and oven dried at 40 °C.

Stable Isotopes: CaCO₃ analyses were carried out on bulk sediment samples in a UIV Inc. Coulometrics Coulometer at PSU (Site M0077) and at the University of California, Santa Cruz (UCSC) for all other sites, with a precision of 0.05%. Stable isotope analysis of bulk CaCO₃ was carried out on a Kiel/MAT253 at UCSC. Analytical precision was better than ±0.05‰ for δ¹³C. All values are reported relative to vPDB.

Trace Element Analysis: 400 µg of bulk sediment sample material was homogenized with mortar and pestle, dissolved in 500 µL of optima-grade 0.075 N HNO₃, and mixed with a vortex mixer. To remove the non-carbonate fraction of the bulk sediments, samples were then centrifuged at 5000 rpm for 10 minutes, and the supernatant fluid was transferred to 1N HNO₃-washed (i.e., boron-cleaned) polypropylene vials. Dissolved samples were analyzed for trace, minor, and major elements via inductively-coupled mass spectrometry (ICP-MS) with a Thermo Element XR at UCSC, following the analytical methodology of Brown et al. (2011). Inter-run precision was monitored using consistency standards, and was <7% (2sd) for B/Ca during sample runs. [B] is then calculated under the assumption that calcite is the only material supplying boron and calcium to the dissolved sample.

X-Ray diffraction: Powder X-ray diffraction was used to identify the mineral phases in the collected core samples. Bulk sediment samples were air-dried and ground in an agate mortar using an agate pestle. The powder was then mounted on a zero-background quartz plate, and XRD data were collected with a PANalytical X'Pert Pro MPD at PSU at 45 kV and 40 mA using a Cu target ($\lambda = 5.1418 \text{ \AA}$) and a solid-state hybrid pixel detector. Powdered samples were scanned from 5° to 70° 2-theta at 2 deg/min. The incident beam passed through a 1/4° divergence slit, a 1/2° anti-scatter slit, and 0.04 rad Soller slits. The diffracted beam passed

Table 1

Definition and thickness of the micrite layer at the study sites. + indicates minimum thickness. Mic/sphere is relative abundance of dispersed micrite and translucent spheroids.

Site	Hole	Location	Base	mbsf	Top	mbsf	Thickness	# Slides	mic/sphere
M0077	A	Chicxulub Crater	40R-1, 108	617.32	40R-1, 34	616.58	0.74	95	mostly micrite
95		Yucatan Outer Basin	13R-3, 36	398.36	13R-1, 113	396.13	2.23+	23	mostly micrite
208		Lord Howe Rise	33R-1, 63	576.63	33R-1, 33	576.33	0.3	33	mostly micrite
356		Sao Paulo Plateau	29R-3, 33	411.83	29R-3, 28	411.78	0.05	27	all spheres
384		J-Anomaly Ridge	13R-3, 32	167.92	13R-3, 0	167.6	0.32	30	mixture
465A		Hess Rise	3R-3, 115	62.15	3R-3, 90	61	0.25	14	mostly spheres
528		Walvis Ridge	31R-CC	407.27	31R-6, 80	405.8	1.47+	9	mixture
536		Camppech Escarpment	9R-5, 145	77.95	9R-5, 28	76.78	1.17	21	mixture
690	C	Maud Rise	15X-4, 39	247.79	15X-4, 16	247.56	0.23	39	mixture
738	C	Kerguelen Plateau	20R-5, 102	377.22	20R-5, 40	376.6	0.62	57	mixture
752	B	Broken Ridge	11R-3, 93	358.73	11R-3, 13	357.93	0.8	38	mixture
761	C	Exmouth Plateau	3R-3, 75	172.47	3R-3, 55	172.27	0.2	39	mixture
999	B	Colombia Basin	60R-1, 50	1050.6	59R-2, 118	1048.18	2.42	12	mixture
1001	A	Nicaragua Rise	38R-CC, 21	352.25	38R-CC, 4	352.08	0.17+	4	mixture
1049	A	Blake Nose	17X-2, 19	125.49	17X-2, 49	125.79	0.3	9	mixture
1124	C	Rehoku Drift	48X-CC, 9*	463.28	48X-CC, 3	463.22	0.06+	14	mixture
1138	A	Kerguelen Plateau	52R-3, 129	490.99	52R-2, 120	489.4	1.59	36	mixture
1209	A	Shatsky Rise	25H-6, 109	235.29	25H-6, 103	235.23	0.06	12	mostly spheres
1210	A	Shatsky Rise	24H-4, 45	219.85	24H-4, 38	219.78	0.07	10	mostly spheres
1259	B	Demerara Rise	13R-1, 49	445.19	13R-1, 26	444.96	0.23	45	mixture
1260	A	Demerara Rise	36R-4, 94	332.14	36R-4, 55	331.75	0.39	43	mostly spheres
1262	B	Walvis Ridge	22H-4, 137	195.53	22H-4, 0	194.16	1.37	59	mixture
1267	B	Walvis Ridge	32X-4, 84	286.34	32X-3, 52	284.52	1.82	25	mixture
TN, Campos Basin			166	39			1.27	30	mixture
Lajilla, Mexico			0-2	+195-200			2.00+	15	mostly micrite
Brazos, Texas	Hansen		-15.18	-9.98			5.2	23	mostly spheres
El Kef, Tunisia	A		16-1, 110	20.08	16-1, 34	19.32	0.76	14	mostly spheres
Stevns Klint, Denmark			2-1	0	6-2t	0.24	0.24+	12	mixture
Beloc, Haiti			0	17.95			17.95+	15	mostly micrite
Gorgonilla Island			G-18, 88	18.88	G-20, 73	20.73	1.85	8	both micrite and spheres
YAX Core, Chicxulub			1272	793.94	1270	793.35	0.59	7	mostly micrite

through a 1/4° receiving slit, 0.04 rad Soller slits, and a Ni filter. Phase identification and phase abundance from all XRD patterns were performed using Jade 2010 Analysis software by MDI of Livermore, CA. Results are shown in Supplemental Materials Table 1.

Biomarker analyses: Total lipid extracts were obtained via Accelerated Solvent Extraction of approximately 12.5 g of bulk sediment and dried to <1 mL under a stream of N₂. Lipid extracts were separated into fractions (aliphatics, aromatics, and polars) via Accelerated Solvent Extraction as per Magill et al. (2015). Mobile phases of 100% hexane, 85% hexane /15% methylene chloride, and 70% methylene chloride / 30% methanol (volume: volume) were used to separate the aliphatic, aromatic, and polar fractions respectively. Lipid fractions were brought to near dryness under a stream of N₂. Aliphatic fractions were analyzed via GC-MS on a Thermo Scientific Trace 1310 Gas Chromatograph coupled to a Thermo Scientific ISQ LT single quadrupole Mass Spectrometer at PSU via 1/10 manual injections. A Restek Rtx-1 fused silica column (60 m length x 0.25 mm ID x 0.25 μm df) was used with a helium carrier gas. The oven program started with an injection temperature of 40 °C held for 1.5 minutes, followed by a rise of 15.0 °C/min until temperature reached 140 °C, after which temperature increased 2.0 °C/min until temperature reached 320 °C, from which time the temperature was held for 20 minutes. 100% of flow was transferred to the ISQ quadrupole mass spectrometer, transfer line temperature 320 °C, and electron ionization 230 °C, which scanned for four scan filters: (1) a mass range of 43-800 Daltons at 5 scans/s, (2) selected ion monitoring of mass 191 amu at 5 scans/s, (3) selected ion monitoring of mass 217 at 5 scans/s, and (4) selected ion monitoring of mass 218 at 5 scans/s. Biomarker quantifications were determined from MS peak area, using ACSO standard oil, Macondo oil, and an n-C₁₀ to n-C₄₀ alkane standard and response curve. Mass spectra were used for compound identification by comparison with standards and published spectra.

Age control of sites: The study sites have a variety of published stratigraphic controls: planktic foraminifera and calcareous nannofossil biostratigraphy, orbital stratigraphy and magnetostratigraphy. In the immediate boundary interval, several sites have measured Ir anomalies (465A, 690, 738, 752, 761, Beloc, Brazos, Fish Clay, El Kef, Lajilla). Biostratigraphic age control was obtained over many years of investigation and is of variable quality. Nannofossil assemblages show distinct hemispheric disparities with Danian species appearing earlier at Northern Hemisphere sites (Jiang et al., 2010) and a sequence of “boom-bust” taxa showing significant diachroneity (Jones et al., 2019). Planktic foraminifera generally recovered faster than calcareous nannoplankton (Hull et al., 2011; Lowery et al., 2018) and show a more consistent sequence of markers that can be applied for biostratigraphy. The earliest Danian P0 Zone, however, is typically missing at open ocean sites, hindering global correlation. Moreover, distinctly different assemblages are observed at high-latitude sites (Huber, 1991), complicating the correlation with lower-latitude locations.

Because of the difficulties with traditional microfossil biostratigraphies, the most accurate correlation in the K-Pg interval involves magnetostratigraphy and orbital stratigraphy. Magnetostratigraphy does not provide good resolution as the boundary lies within Chron 29r and the Chron 29r/Chron29n boundary lies 368 kyr above it (Westerhold et al., 2008). Thus orbital stratigraphy provides the most accurate time control and is used here to obtain age estimates for the duration of the micrite-rich bed. Unfortunately, orbital age control is only available at more recently drilled sites, including Sites 1001 (Röhl et al., 2001), 1209, 1210, 1262 and 1267 (Westerhold et al., 2008). Our estimates for the range of the duration of the micrite-rich bed are based on Sites 1210 and 1262 with sample ages shown in Westerhold et al. (2008) and Jones et al. (2019).

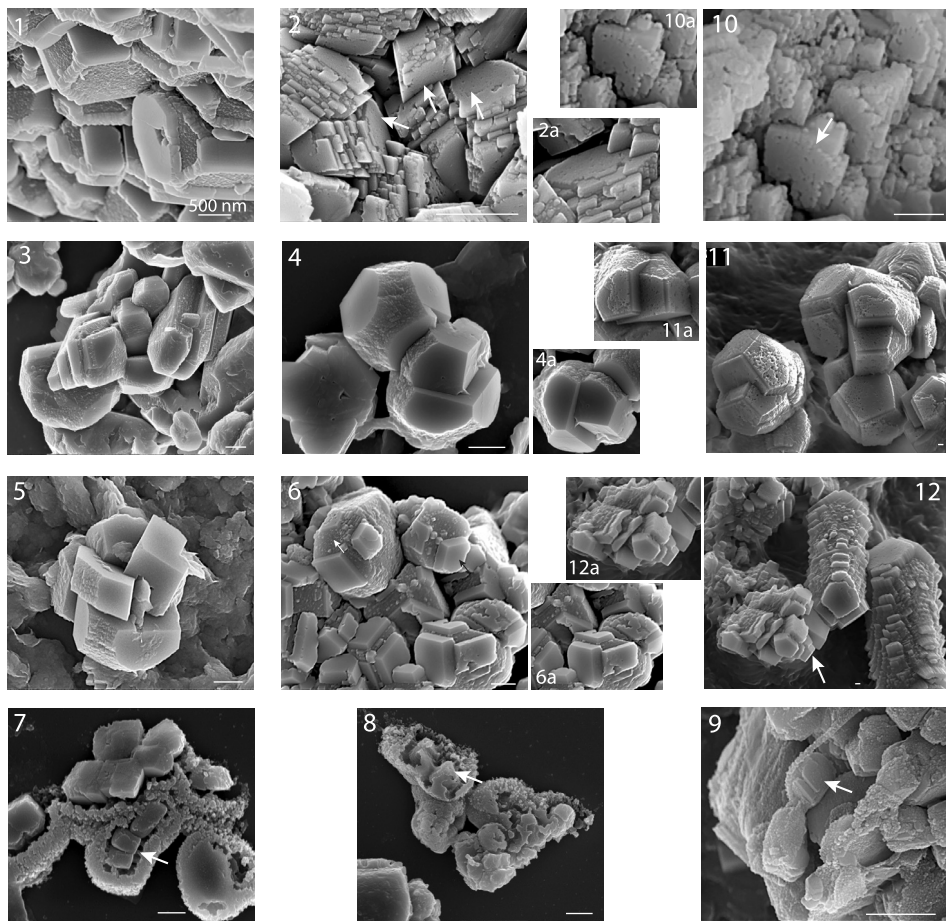


Fig. 2. Morphology of micrite structures (Pl. 1-9) compared to calcite produced by modern bacterial species from natural environment (Pl. 10) and in culture (Pl. 11, 12). Pl. 1. Modified scalenohedral microcrystals showing mesocrystals; Pl. 2. Rhombohedral microcrystals showing mesocrystals, arrows show porous faces; Pl. 3. Complex rhombohedral microcrystals showing mesocrystals; Pl. 4, 5. Scalenoclusters showing mesocrystals; Pl. 6. Modified scalenohedral microcrystals showing mesocrystals and flat crystal faces; Pl. 7, 8. Capsular rhombohedra, internal crystals shown with arrows; Pl. 9. Possible capsular rhombohedra; Pl. 10. Rhombohedral mesocrystals produced by modern stromatolite cyanobacteria after Paclt et al. (2015) (arrow shows porous faces (compare to structure in Pl. 2)); Pl. 11, 12. Scalenoclusters produced by *Streptomyces luteogriseus* in culture after Cao et al. (2016) (arrow in Pl. 12 shows flat and porous faces). Striking modern-ancient morphology resemblance shown in small plates that identify key features: porous plates—Pl. 2a compare with Pl. 10a; scalenocluster—Pl. 4a compare with Pl. 11a; smooth and mesocrystal faces—Pl. 6a compare with Pl. 12a. Pl. 1. Sample 1262B-22-4, 134 cm; Pl. 2. Sample 1210A-24H-4, 40 cm; Pl. 3. Sample 761C-3R-3, 67 cm; Pl. 4. Sample 1259B-13R-1, 30 cm; Pl. 5. Sample 1262B-22-4, 30 cm; Pl. 6. Sample 690C-15X-3, 22 cm; Pl. 7, 8. Sample 465A-3R-3, 105 cm; Pl. 9. Sample 1210A-24H-4, 38 cm; Pl. 10-12 reproduced with Creative Commons CC-BY licenses. Scale bar represents 500 nm.

3. Results

Smear slide observations suggest that microcrystalline calcite (also known as micrite) is the dominant carbonate component directly above the K-Pg boundary at all 31 sites. The thickness of the micrite-rich carbonate layer ranges from 0.06 to over 17.95 meters (Fig. 1; Table 1), and generally is greater in sections closer to the impact, possibly due to redeposition by high-energy processes including gravity flows and tsunami (e.g., Bralower et al., 1998). Its basal part in more expanded sections contains rare (< 5%) surviving and reworked Cretaceous calcareous nannofossils with rare fragments and whole specimens of planktic foraminifera. Planktic foraminiferal abundance increases upwards and calcareous dinoflagellates (calcispheres), dominated by the disaster taxon *Cervisiaella*, gradually appears in the middle of the layer. They are joined by the common, largely disarticulated disaster nannoplankton taxa *Braarudosphaera* and *Biantholithus* at South Atlantic and some Gulf of Mexico sites. The top of the layer is difficult to define, because the abundance of micrite gradually declines upward, and incoming Danian nannofossils, including the dominant so-called “boom bust” species (Bown, 2005; Jones et al., 2019), *Braarudosphaera*, calcispheres, and foraminifers gradually increase in abundance. Thus the layer thickness is somewhat arbitrary (Supplemental Materials Section 3), especially at sites where subsidiary

Braarudosphaera, *Biantholithus* and abundant calcispheres supply dispersed micrite. The layer contains variable amounts of clay, encompassing the traditional K-Pg “boundary clay” in condensed sections, and lithic material at proximal sites.

Field emission-scanning electron microscopy (FE-SEM) shows that well-preserved crystals range from sub-micrometer to 5 μ m in size, with a variety of crystal forms including rhombohedra, modified scalenohedra and complex geometries that are difficult to characterize (Figs. 2, 3; Supplemental Materials Figures 1, 2). These micron-sized crystals, termed microcrystals here, are commonly composed of highly regular, rhombohedral subcrystals \sim 5–20 nm in size (e.g., Fig. 2; Pl. 1–3; Supplemental Materials Figure 1; Pl. 1–6), and are commonly referred to as mesocrystals (e.g., Colfen and Antonietti, 2005). Well-preserved specimens are rare and generally only identifiable in the FE-SEM. Even in the FE-SEM most micrite is generally smooth and featureless with over 200 hours devoted to observing specimens. Distinct microcrystals are observed at numerous sites (Fig. 1), but preservation is better at some (Sites 465, 1210, 1262) where we focused efforts.

Transmission electron microscope (TEM) observations (Ocean Drilling Program (ODP) Sites 738 and 1262) show rhombohedral and trapezoidal CaCO_3 microcrystals less than 1 μm in size and 50 nm mesocrystals of calcite encased in clay (Fig. 4; Pl. 1–6). X-ray diffraction of assorted samples from the micrite layer, including

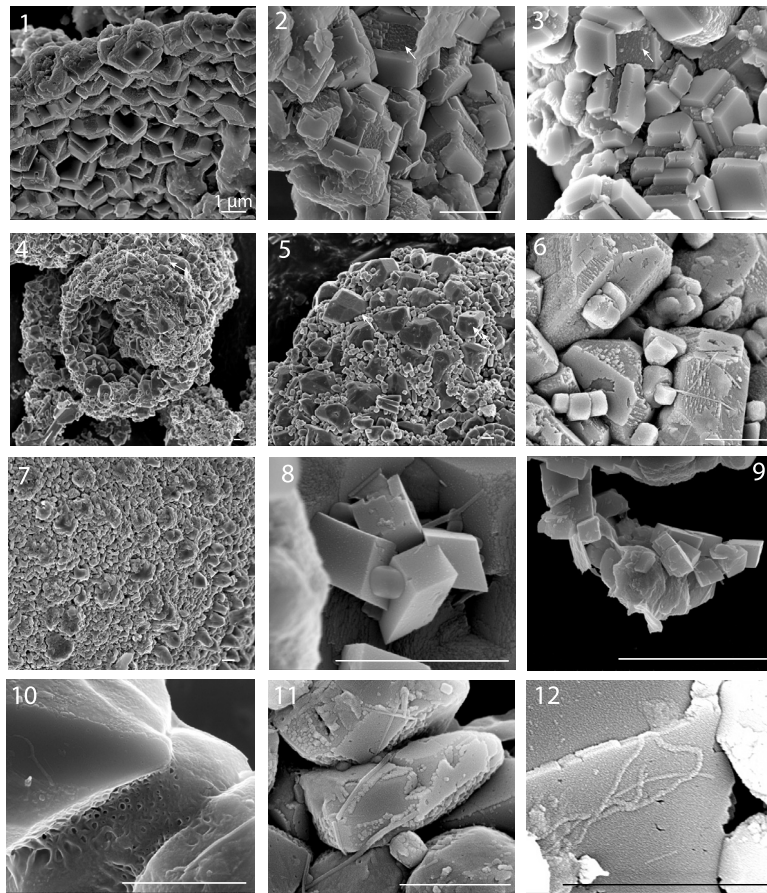


Fig. 3. Morphology of micrite structures (Pl. 1-9) and biological structures (Pl. 10-12). Pl. 1, 2. Internal wall of shelled scalenohedra; Pl. 3. External wall of shelled scalenohedra (white arrows in Pl. 2, 3 show incompletely evolved or pitted face bearing mesocrystals; black arrows show highly developed, smooth face); Pl. 4, 5. Planktic foraminiferal chamber made of modified scalenohedral microcrystals (both specimens are quite overgrown; arrows show well preserved microcrystals); Pl. 6. Modified scalenohedral microcrystal from same specimen as Pl. 4. Pl. 7. Microperforate foraminiferal wall texture showing raised areas or pustules; Pl. 8, 9. Rhombohedral microcrystals without mesocrystals; Pl. 10-12. EPS-like structures. Pl. 1, 2, 6. Sample 1210A-24H-4, 39 cm; Pl. 3, 4. Sample 1262B-22H-4, 134 cm; Pl. 5. Sample 690C-15-X-3, 22 cm; Pl. 7. Sample 1049C-8X-7, 72 cm; Pl. 8, 9. Sample 1210A-24H-4, 38 cm; Pl. 10. Sample 1210A-24H-4, 37 cm; Pl. 11, 12. Sample 1210A-24H-4, 40 cm. Scale bar represents 1 μm .

that in the transitional unit at Site M0077, shows that CaCO_3 in the layer is exclusively calcite (Supplemental Materials Table 1).

B/Ca measurements of the bulk carbonate fraction in the boundary interval at six sites are associated with a positive anomaly (Fig. 5) ranging in size from <300 (Site M0077) to >10,500 (Site 1262) $\mu\text{mol/mol}$. Hopanes and steranes were abundant in samples from Sites 738 and 1262, but 2α -methyl hopanes are at or below detection limits (Fig. 6).

4. Discussion

4.1. A global microcrystalline calcite bed formed in the impact aftermath

Micrite above the K-Pg boundary has been described from several deep sea sites (Thierstein et al., 1991; Bralower et al., 2002; Bown, 2005; Minoletti et al., 2005; MacLeod et al., 2007), but we are the first to suggest that it is an ocean-wide feature of the K-Pg boundary record. This micrite-rich carbonate layer can be placed in the temporal sequence of impact-related materials. At “ground zero,” in the Chicxulub crater (Site M0077), micrite was deposited in waters of ever lessening turbidity as the activity of seiche waves within the crater gradually subsided (Lowery et al., 2018; Gulick et al., 2019), below the Ir anomaly (Goderis et al., 2019). At Beloc (Haiti), Brazos (Texas), and Lajilla (Mexico), abundant micrite occurs in impact spherule-bearing units, deposited under high-energy conditions. At some other locations globally, the micrite-rich layer contains charcoal and other burn markers (Sites

M0077, 738, 1210 and 1262; Gulick et al., 2019; Lyons, 2020, in press; Supplemental Materials Figure 3). The occurrence of charcoal, spherules and the Ir anomaly in the lower part of the carbonate bed suggests that micrite deposition began in the immediate aftermath of the impact (Kring and Durda, 2002), possibly within days to years at proximal sites. The top of the layer is hard to define, as discussed, but deposition of micrite at some but not all sites extends above the base of the globally synchronous negative carbon isotope excursion that characterizes the K-Pg boundary (e.g., Zachos and Arthur, 1986) (Fig. 5), suggesting that the top of the layer is asynchronous. This asynchronicity is confirmed by orbital stratigraphy (Westerhold et al., 2008) which provides a range from 46 kyr post boundary at Site 1210 up to as late as 250 kyr at Site 1262 (equivalent to planktic foraminiferal Zone P α to P1a at least). Regardless of its variable stratigraphical extent, the micrite-rich carbonate layer is consistently present and therefore a global feature of the K-Pg boundary. In the following, we explore the morphology of the micrite crystals then probe the significance of the layer in relation to the ocean chemistry, environment and ecology of the boundary interval.

4.2. Morphology of micrite microcrystals

The gross morphology of the micrite crystals (Minoletti et al., 2005) has been previously described, but their size, form and texture have not been studied at high resolution which requires field emission scanning electron microscopy. In fact, imaging of calcite

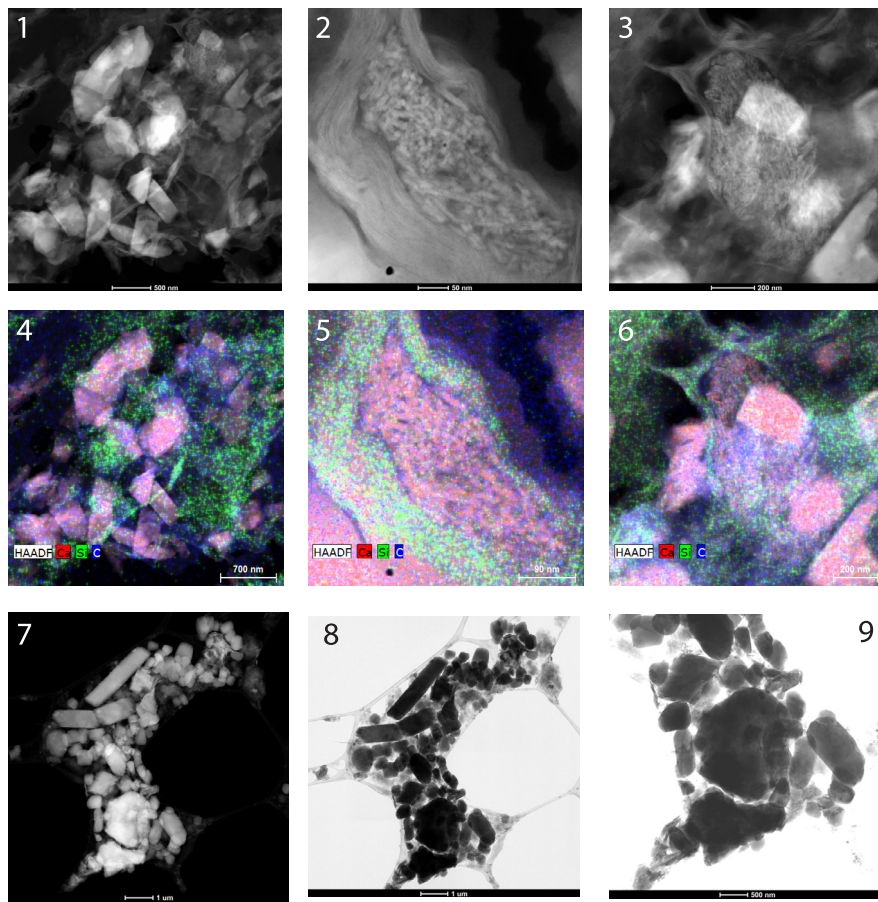


Fig. 4. Transmission electron micrographs and EDXS maps. Pl. 1-3 STEM images of Sample 738C-20R-5, 91 cm showing array of forms and mesocrystals. Pl. 4-6 EDXS maps of views in Pl. 1-3 with Si-green, C-blue, Ca-red. Pl. 7-9. STEM images of Sample 1262B-22H-4 134 cm showing rhombohedral and trapezoidal crystals (thin strands are copper grid). Scale bars in individual images.

in deep-sea sediments at sub-micrometer resolution is rare, making our observations novel, and sometimes puzzling. They reveal rare crystals with nm-scale structures that are surprisingly pristine given their age. Where well preserved, the micrite is largely composed of isolated microcrystals or clusters of microcrystals which show a considerable degree of morphologic variation. Crystal form is highly variable, but we infer four distinct microcrystal arrangements from well-preserved specimens (Table 2): (1) clusters of four to six modified scalenohedra, hereafter termed “scalenoclusters” (Fig. 2; Pl. 4, 5; Supplemental Materials Figure 1; Pl. 7-12); (2) clusters of multiple rhombohedra or more complex geometries of highly variable size and shape, termed “rhomboclusters” (Fig. 2; Pl. 2, 3; Fig. 3; Pl. 8, 9; Supplemental Materials Figure 2; Pl. 5-15); (3) one to three small rhombohedra enveloped in a delicate, porous capsule, termed “capsular rhombohedra” (Fig. 2; Pl. 7-9; Supplemental Materials Figure 2; Pl. 1-4); and (4) delicate shell walls made of poorly-organized modified scalenohedra, termed “shelled scalenohedra” (Fig. 2; Pl. 1; Fig. 3; Pl. 1-6; Supplemental Materials Figure 1; Pl. 5, 6). Well-preserved microcrystals in all groups show highly developed, smooth faces and edges, usually alternating with incompletely evolved faces that display internal mesocrystals, giving them a pitted appearance (Fig. 2; Pl. 6; Fig. 3; Pl. 2, 3). Rhomboclusters include agglomerates of interlocking crystals with and without mesocrystals (Fig. 3; Pl. 8, 9; Supplemental Materials Figure 2; Pl. 5-14). These crystals are also found as overgrowth on coccoliths (Supplemental Materials Figure 4; Pl. 4-9).

Shelled scalenohedra derive largely from small (<63 µm and often < 30 µm) planktic foraminifera (Fig. 3; Pl. 1-6; Supplemental Materials Figure 5; Pl. 5-12), and represent a novel wall structure

for this group which typically has a microcrystalline, porous texture with pustules and spines (Fig. 3; Pl. 7; Supplemental Materials Figure 5; Pl. 1-4). A range of preservational states is observed from pristine (Fig. 3; Pl. 1-3) to annealed and heavily overgrown (Fig. 3; Pl. 4-6). Modified scalenohedral microcrystals are loosely bound in foraminifera as indicated by cross-polarized light microscopy which shows common translucent foraminiferal fragments that disintegrate into dispersed microcrystals (Supplemental Materials Section 1) and Supplemental Materials Figure 6; Pl. 1-5; Supplemental Materials Figure 7; Pl. 7-9). Not all translucent spheres are made of microcrystals, however; earliest Danian foraminifera are thin-walled, especially juvenile forms, and such specimens appear translucent in smear slides.

Overall, the fragility of microcrystals and their common overgrowth limits assignment of the majority of specimens to one of the four microcrystal arrangements, thus their relative contributions to each type cannot be determined. However, there appear to be at least qualitative differences in abundances among sites (Supplemental Materials Section 3). For example, at some tropical and shelf sites (El Kef, 465A, 1209, 1210, 1259, 1260), abundant translucent shell fragments, possibly pieces of shelled scalenohedral foraminiferal tests, occur without significant dispersed micrite (Fig. 1; Table 1).

Rare occurrences of near pristine micrite preserve potential biological structures: < 50 nm wide filaments and networks of strands resembling extracellular organic materials observed in modern biofilms (Fig. 3; Pl. 10-12; Supplemental Materials Figure 8; Pl. 1-12). These structures are generally too small to be bacterial cells, but in size and shape resemble extracellular structures (such as

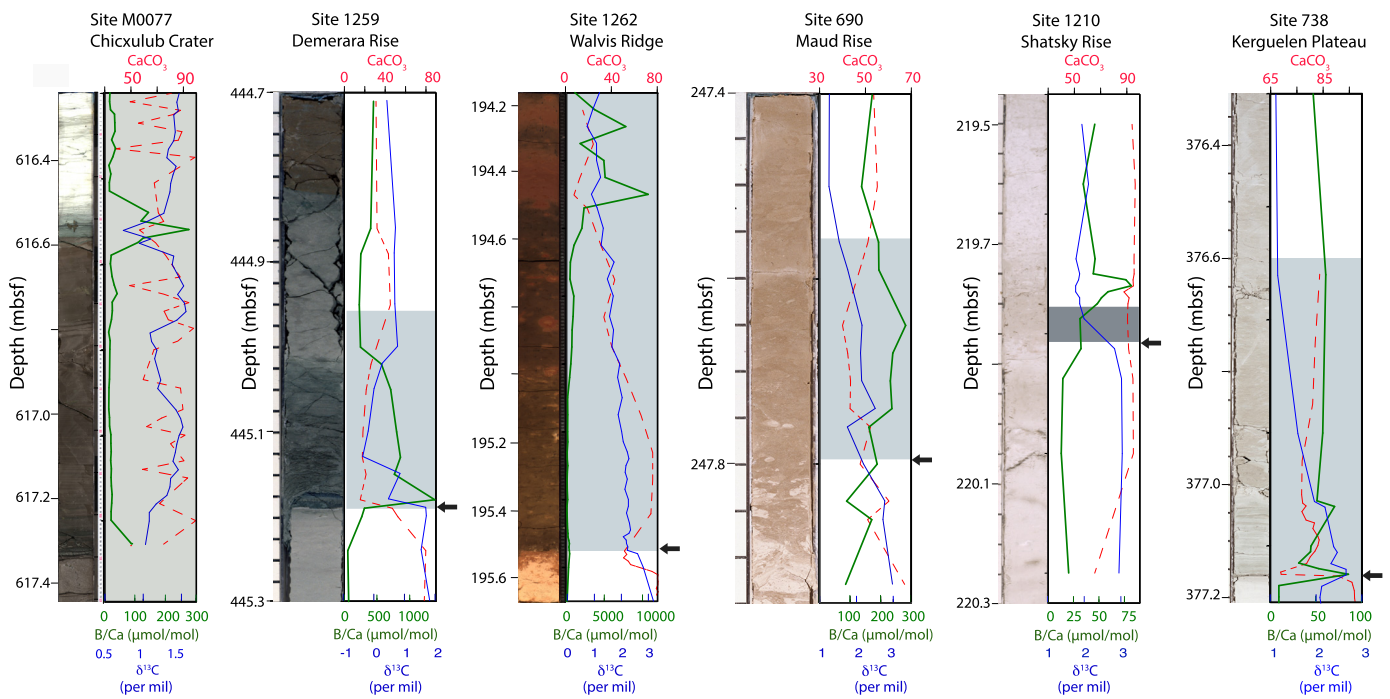


Fig. 5. B/Ca values (green thick line), C-isotopes (blue thin line) and %CaCO₃ content (red dashed line) from six sections crossing the K-Pg boundary. Location of paleontological boundary shown with arrow. Location of micrite-rich layer shown with color panels, nature of micrite as in Fig. 1.

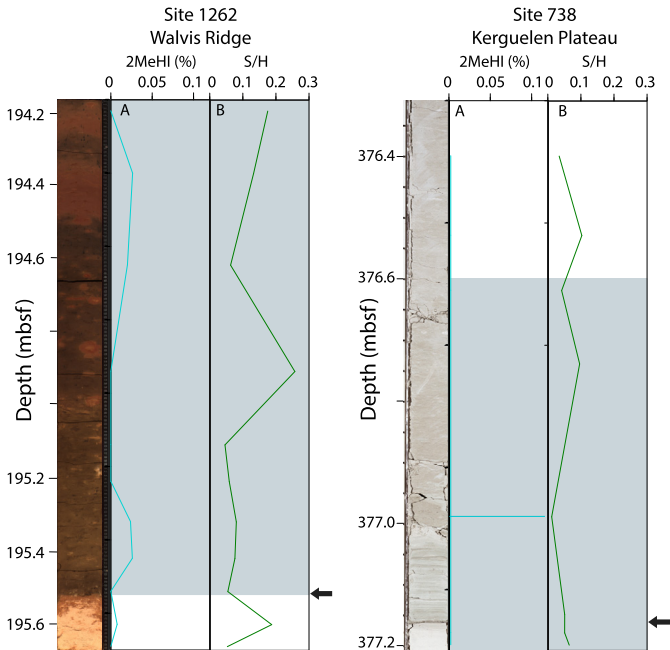


Fig. 6. Biomarker data from Sites 738 (Kerguelen Plateau) and 1262 (Walvis Ridge). A. 2-methyl hopane index (2MeHl%) indicative of cyanobacteria (light blue line); B. Sterane/Hopane ratio (S/H) indicative of the relative contribution of bacteria (H) and algae (S) (green line). See text for discussion. Location of paleontological boundary shown with arrows. Location of micrite-rich layer shown with color panels, nature of micrite as in Fig. 1.

Extracellular Polymeric Substances, EPS) of bacteria or algae. Most filaments lie on the surfaces of crystals, but they appear to be exclusive to grains composed of mesocrystals, indicating that filaments were original and not derived during burial or sample sputtering.

4.3. Origin of the global micrite-rich layer in the aftermath of the K-Pg mass extinction

We have shown that the K-Pg micrite-rich layer is largely micrite, and where well preserved, contains an array of crystal forms and surface textures. Morphology is just one attribute that can be used to differentiate the origin of calcite crystals, in particular whether they are biological in origin (i.e. biominerals) (e.g., Weiner and Dove, 2003). With this understanding in mind, we attempt to distinguish between the potential origins in part based on comparison of the morphology of microcrystals with natural and experimental samples, and, where applicable, based on geochemical data. We acknowledge from the outset that such interpretation can be difficult because biomineralization may be intimately associated with inorganic precipitation in nature, and abiotic precipitates can mimic biological materials (e.g., Schopf et al., 2010). Moreover, materials within the four microcrystal arrangements are highly variable and may have more than one origin. We consider four possible origins for the micrite in the global layer: diagenetic reprecipitation of calcite (e.g., Fabricius, 2007), backreaction of CaO formed by volatilization of target limestone (Yancey and Guillemette, 2008; Schulte et al., 2009), chemical precipitation from oversaturated seawater (e.g., Caldeira and Rampino, 1993; Henehan et al., 2016), and precipitation controlled or induced by cyanobacteria or non-haptophyte microalgae. An essential element of our interpretation is the occurrence of the mesocrystals, which represent rapid crystal growth via particle aggregation, also known as crystallization by particle attachment (CPA) (De Yoreo et al., 2015; Gilbert et al., 2019). Mesocrystals are widely reported in rapidly precipitated biogenic calcite, but can also be abiotic, for example in calcite precipitated in hot springs and numerous phases grown in experiments (e.g., Seto et al., 2012; Goetz et al., 2014; Cuif and Dauphin, 2005; Peng and Jones, 2013; Casella et al., 2018).

4.3.1. Diagenetic reprecipitation

Micrite is common in pelagic sediments, and can be formed via post-biogenic processes of dissolution and reprecipitation of diagenetic carbonate. This material forms largely via dissolution of

biogenic materials followed by precipitation in pore waters (e.g., Scholle, 1977). The process is widely considered to be geologically slow and typically fills pore space. Diagenetic calcite is thus generally anhedral with a smooth, featureless surface texture in the SEM (e.g., Pérez-Huerta et al., 2018). Below the K-Pg boundary, we observe predominantly irregularly shaped, larger micrite crystals that we link to diagenetic formation in the pore spaces (Supplemental Materials Figure 9; Pl. 1-3). Rhombohedral calcite crystals are rarely produced via diagenesis unlike dolomite. Most likely, such crystals are direct overgrowth on biogenic rhombohedral grains such as elements of coccoliths (Fabricius, 2007), which we observe in the carbonate layer (Supplemental Materials Figure 4; Pl. 4-9). Precipitation is slow and ordered, and likely via ion-by-ion addition (e.g., Colfen and Antonietti, 2005), so that mesocrystals are unknown in diagenetic calcite. Moreover, experimental alteration of biogenic materials shows that reprecipitation of biogenic calcite removes the mesocrystal structure (Casella et al., 2018), and fossil materials altered by diagenesis are generally featureless at the nanometer scale (Pérez-Huerta et al., 2018). Some rhombocluster specimens appear smooth (Fig. 3; Pl. 8), but most show at least some evidence of mesocrystals (Supplemental Materials Figure 2; Pl. 5-15), suggesting rapid precipitation. Overgrown foraminiferal tests formed of modified scalenohedral microcrystals (e.g. Fig. 3; Pl. 4, 5; Supplemental Figure 5; Pl. 6-11) can also be distinguished from diagenetically overgrown foraminiferal tests, which are not composed of mesocrystals (Supplemental Figure 5; Pl. 1-5). We therefore conclude that the majority of microcrystals in the K-Pg boundary sites are not diagenetic in origin (see Supplemental Materials Section 2 for more information). Some of the rhombohedral crystals, especially crystal overgrowths (Supplemental Materials Figure 4; Pl. 4-9), however, may have grown during the early stages of burial when pore spaces were relatively open and crystal growth was unconstrained. Moreover, we postulate that dissolution during organic matter oxidation may explain the lack of micrite in shelf locations such as El Kef.

4.3.2. Backreaction of CaO

At pressures associated with an impact, limestone dissociates into CaO and CO₂ (Yang and Ahrens, 1998). CaO could have back-reacted with CO₂ in the vapor plume, ejecta curtain, or with ambient CO₂ in the atmosphere or seawater, to reprecipitate CaCO₃ (Agrinier et al., 2001; Cizer et al., 2012). Rounded carbonate clasts in K-Pg boundary deposits on the Demerara Rise (Sites 1259 and 1260) and at Brazos are thought to have been formed via back-reaction (Yancey and Guillemette, 2008; Schulte et al., 2009); the microtexture of calcite at Site M0077 (Bralower et al., *in review*) suggests that the majority of dispersed rhombohedral grains in the thick micrite-rich layer in proximal sites (Fig. 1) have the same origin. Because backreaction/carbonation is rapid, it is possible that it would form mesocrystals; indeed the somewhat irregular micro-crystals in Site M0077 samples (Supplemental Materials Figure 1; Pl. 10-12) may have formed via backreaction/carbonation within months of the impact (Bralower et al., *in review*). However, the morphology of calcite produced experimentally by carbonation of Ca(OH)₂ is either amorphous or well-formed scalenohedral (Cizer et al., 2012), thus differs from the majority of crystals described here.

CaO was emplaced in a fast-moving dust cloud that circled the globe (Artemieva and Morgan, 2020), but deposition from this cloud cannot explain the observed thickness of micrite at distal sites. The carbonate within the ejection (transient) cavity covers an area with a radius of ~45 km and thickness of ~3 km. The total volume of this carbonate is equal to $2 \times 10^{19} \text{ cm}^3$ if deposited over the surface area of the Earth ($5 \times 10^{18} \text{ cm}^2$) giving a layer with an average thickness of 4 cm assuming even distribution over the Earth's surface. This thickness estimate is a maximum because

a significant amount of carbonate did not disassociate, and ends up as fragments within impact breccias at the impact site, as well as at proximal sites.

4.3.3. Abiotic precipitation from oversaturated seawater

Reaction of CaO in the oceans consumes CO₂ and leads to an increase in calcite saturation. However, volatilization of the impact target may have led to short-term ocean acidification, likely from rainout of SO₂, NO_x and, to a lesser degree, from CO₂ (Alegret et al., 2012) a prediction validated using boron isotopes (Henehan et al., 2019). Over longer time scales (kyr to hundreds of kyr), decimation of eukaryotic planktonic calcifiers with continuation of (possibly reduced) soft-tissue biological pumping of CO₂ from surface waters, together with continuing riverine delivery of alkalinity, may have increased surface ocean saturation (Boudreau et al., 2018), potentially to levels where calcite precipitated directly from seawater (Henehan et al., 2016). At face value, the B/Ca positive anomaly (Fig. 5) is indicative of an increase in pH (Yu et al., 2007), matching interpretation of a positive B isotope excursion following the brief acidification interval (Henehan et al., 2019). However, the strong overall negative correlation between bulk carbonate B/Ca anomalies and CaCO₃ content at Sites 690, 738, 1259, 1262, and possibly at M0077, indicates that a large fraction of the high B levels is derived from clay (Ishikawa and Nakamura, 1993) (Fig. 5; Supplemental Materials Figure 10), so that we cannot interpret these data in terms of pH. The lower B/Ca anomaly (<10 μmol/mol) at Site 1210, however, shows no correlation with CaCO₃. This anomaly corresponds to the interval of peak micrite content and may indicate an increase in local surface ocean pH and saturation (Uchikawa et al., 2015), the CaCO₃ "overshoot" about 46 kyr after the K-Pg boundary (the B isotope peak at Site 1209 is 54 kyr after the boundary (Henehan et al., 2019)) (see Supplemental Materials Figure 11). Although the boron data do not indicate that the surface ocean became oversaturated to the point where calcite precipitated directly from seawater in the immediate aftermath of the boundary, we cannot discount the possibility that the simple rhomboclusters and the moderately abundant, small (<1 μm) dispersed rhombohedral grains of calcite found at numerous sites (Supplemental Materials Figure 7; Pl. 1-6) are abiotic in origin. Indeed, the agglomerates of interlocking rhombohedra, or rhomboclusters (Fig. 3; Pl. 8, 9; Supplemental Materials Figure 2; Pl. 6-15) observed at Sites 738, 1210 and 1262 resemble synthetic calcite (e.g., Lemarchand et al., 2004; Heberling et al., 2011), and the 1210 samples overlap with the peak in B/Ca. One instance of agglomerates growing around a piece of charcoal (Supplemental Materials Figure 2; Pl. 11-12; Supplemental Materials Figure 3; Pl. 9, 10) could be interpreted as resulting from precipitation in surface waters as charcoal would settle slowly allowing for crystals to grow. However, this and other agglomerates could represent a continuum of precipitation from surface waters to the top of the sediment column. In general, these rhomboclusters are without mesocrystals, but there are exceptions (Supplemental Materials Figure 2; Pl. 14, 15).

4.3.4. Precipitation induced or influenced by bacteria and non-haptophyte algae

Today, aragonitic and calcitic mesocrystals are commonly precipitated by a range of organisms in cultures and the natural environment (Anbu et al., 2016; Han et al., 2017), with rapid growth via CPA commonly producing highly regular, rhombohedral sub-crystals. In fact, this process has produced skeletal materials in a range of animals throughout geologic time (Gilbert et al., 2019). Such precipitation can be biologically mediated through three main processes: (1) biologically directed (or controlled) biomineratization, in which the organisms exert a strong genetic control on the nucleation and growth of the minerals (generally known as

Table 2

Four different microcrystal forms, general crystal size, example illustration, sites observed and inferred origin.

Microcrystal morphology	Crystal size (μm)	Primary figure	Sites observed	Inferred origin
Scalenoclusters	1-4	Fig. 2; Pl. 4, 5; Supplement Figure 1, Pl. 7-12	0077, 465, 690, 738, 761, 1049, 1124, 1138, 1209, 1210, 1259, 1260, 1262, Campos Basin, Stevens Klint	Microbial
Rhomboclusters	0.25-3	Fig. 2; Pl. 2, 3; Fig. 3; Pl. 8, 9; Supplement Figure 2, Pl. 5-12	738, 761, 1210, 1262	Microbial/Abiotic
Capsular rhombohedra	0.25-0.5	Fig. 2; Pl. 7-9; Supplement Figure 2, Pl. 1-4	465, 1210, 1262, Stevens Klint,	Microbial
Shelled scalenohedra	0.5-4	Fig. 2; Pl. 1; Fig. 3; Pl. 1-6; Supplement Figure 1; Pl. 5, 6	690, 1210, 690, 1262 (SEM) and likely more (LM)	Microbial/foraminiferal

biominerals); (2) indirectly induced mineralization via the modification of the surrounding local conditions such as pH or mineral supersaturation states as a result of the cell's metabolism; and (3) biologically influenced (or passive) precipitation of the minerals (commonly known as organominerals) on extracellular organic substances, without a high level of genetic control (Perry et al., 2007; Dupraz et al., 2009; Benzerara et al., 2011). For example, precipitation of calcite or aragonite can be induced by removal of CO₂ during photosynthesis (e.g. during whiting events (Robbins and Blackwelder, 1992)); and/or influenced through nucleation on microbial organic templates such as exopolymeric substances (EPS) (e.g., growth of stromatolites (Dupraz and Visscher, 2005)).

The form and microtexture of well-preserved modified scalenohedral and rhombohedral microcrystals in the global carbonate layer, are almost completely novel in the fossil record. These microcrystals do not resemble any known form of abiotic calcite, but bear a striking resemblance to calcite crystals precipitated by cultured and naturally occurring bacteria (Fig. 2; Pl. 10-12). The common EPS-like filaments (Fig. 3; Pl. 10-12) support a bacterial interpretation. Several morphologic features are particularly diagnostic: (1) four to six crystal scalenoclusters strongly resemble those formed by cultured cyanobacteria (Fig. 2; compare Pl. 4/4a with Pl. 11/11a); (2) clusters of dozens of rhombohedral and modified scalenohedral crystals, including those preserved in foraminiferal shells, contain flat, porous faces that strongly resemble the exterior of mesocrystals precipitated by cyanobacteria (Fig. 2; compare Pl. 2/2a with Pl. 10/10a); (3) highly developed smooth faces alternating with those that display mesocrystals show a striking resemblance to carbonates precipitated by cultured cyanobacteria (Fig. 2; compare Pl. 6/6a with Pl. 12/12a); and (4) delicate spherical capsules containing internal microcrystals (Fig. 2; Pl. 7-9) resemble cyanobacteria or other bacteria encrusted with fine extracellular carbonate grains and filled with micron-sized, intracellular carbonate (Couradeau et al., 2013). Finally, we note that the calcite crystals within the micrite-rich layer often exhibit "reversed growth" textures. Whereas classical growth models account for the development of apices and edges before faces (Bravais, 1866), as seen in skeletal crystals, the micritic calcite crystals here frequently show well-developed faces and poorly evolved edges (Fig. 2; Pl. 4, 6). These textures resemble those described in travertine (Greer et al., 2017; Jones, 2017b), in which polycrystalline cores were succeeded by single-crystal faces. Greer et al. (2017) invoke a mechanism by which the assembly of mesocrystals is mediated by biomolecules, as reproduced in experiments involving chitosan. Diagnostic specimens resembling cyanobacteria are found throughout the micrite-rich layer, notably with the lowermost sample 3 cm above the boundary at Site 1262.

The modern cyanobacterial crystal examples illustrated (Fig. 2) are larger than the proposed K-Pg microbial crystals, but modern

bacterial precipitates show significant variety in size, with calcite microcrystals between 2 and 5 μm in some instances (Arp et al., 1999; Bang et al., 2001; Jones, 2017a; Jones and Renaut, 2017); the K-Pg specimens are within this range, although at the lower end. The size of microbial calcite is related to saturation state and organic content (Golubic et al., 1999; Meldrum and Hyde, 2001) and thus the relatively small microbial precipitates may have been a response to the environmentally variable post K-Pg ocean. Moreover, from shape alone, we cannot differentiate between the possibilities that the microcrystals were skeletal products whose precipitation was directly controlled by the organism, or materials whose precipitation was induced or influenced via cells' metabolism or reactions with organic matter in and around the cell. We speculate, however, that the forms resembling foraminifera (shelled scalenohedral) were not formed through controlled biominerization because of the difference from the typical shell structure. Regardless of mechanism, the microcrystal form is strong evidence for a microbial origin.

Organic biomarkers can provide additional clues as to which organisms produced these putative microbial precipitates, although there are no diagnostic compounds for calcifying cyanobacteria. The abundance of hopanes and steranes in samples from Sites 738 and 1262 suggests that bacterial and algal production recovered rapidly after the impact, as proposed by Sepúlveda et al. (2009) for Stevens Klint, Denmark. In all localities, the low abundance of steranes relative to hopanes (S/H, Fig. 6) suggests that bacterial productivity outpaced that of eukaryotic algae, or that microbial biodegradation was extensive (Bobrovskiy et al., 2019), or both. The occurrence of 2 α -methyl hopanes is commonly used to signify the presence of cyanobacteria. While 2 α -methyl hopanes are not exclusively produced by cyanobacteria, these organisms are typically considered the major source of 2 α -methyl hopanes. The abundance of 2 α -methyl hopanes at Stevens Klint (Sepúlveda et al., 2009), combined with heterocyst glycolipids (albeit low in abundance) in the transitional unit at Site M0077, are indicative of thriving cyanobacterial communities (Schaefer et al., 2020). However, 2 α -methyl hopanes are at or below detection limits at Sites 738 and 1262 (Fig. 6). This scarcity of cyanobacterial biomarkers may signify that cyanobacteria at open-ocean locations were either absent or, like contemporary taxa in these settings, did not produce 2 α -methyl hopanes. Further, surface waters were likely well-oxygenated and such conditions are not associated with preservation of organic matter including 2 α -methyl hopanes (Ricci et al., 2014). Because of these preservational issues, our investigation suggests that the morphological fossils may provide a more representative distribution of microbial occurrence, especially at pelagic sites. Thus, based on the combination of morphological and biomarker data, we conclude that most micrite in the carbonate layer at distal sites was likely produced by ocean-wide blooms of

cyanobacteria and algae in the millennia after the K-Pg boundary impact.

4.3.5. Model for the origin of the micrite-rich layer

We thus postulate a combination of sources for the micrite that makes up the carbonate layer including a significant fraction from microbes and contributions from backreaction and abiotic precipitation. We propose that a unique set of conditions in the aftermath of the K-Pg impact was consistent with this mixture. We consider the K-Pg micrite-rich layer analogous to modern “whittings” (e.g., Schultze-Lam et al., 1997), where blooms of cyanobacteria modify surface ocean chemistry and ecology and induce micrite precipitation under supersaturated conditions (e.g., Robbins and Blackwelder, 1992; Thompson, 2000; Obst et al., 2009). Modern whiting events are short-lived and have a local or regional extent, in alkaline lakes and tropical shallow water carbonate settings (Coshell et al., 1998). By comparison, the K-Pg micrite-rich layer has a regional to global distribution and a much longer duration, albeit possibly produced by multiple episodic or seasonal events. This timing, and the duration and extent of deposition raise significant dilemma.

Cyanobacterial blooms in whittings require CaCO_3 supersaturation, a condition that is difficult to explain in the nutrient rich (Jones et al., 2019), immediate post-impact interval. However, decimation of the calcareous nannoplankton, the dominant haptophytes in the Cretaceous, and their replacement by dinoflagellates and diatoms (e.g., Knoll and Follows, 2016) would have altered the flux of CaCO_3 relative to organic carbon (C_{org}) out of the surface ocean and caused an increase in saturation over millennia driven by the ongoing input of alkalinity from rivers (Henehan et al., 2016; Boudreau et al., 2018). Sufficiently high levels of supersaturation to initiate whittings (saturation states with respect to calcite > 10) could have been attained only if the eukaryotic- $\text{CaCO}_3/\text{C}_{\text{org}}$ rain rate would have dropped to 50% or 75% (Henehan et al., 2016), which, given the near eradication of calcareous nannoplankton and planktic foraminifera, and the small cell size of survivors (Alvarez et al., 2019), is not unreasonable, even with seasonal or episodic whittings. At that point, whittings would replace the eukaryotic- CaCO_3 flux, increasing the rain ratio, but saturation would remain elevated by riverine influx.

The effect of rain rate on saturation would be offset by lower export production over much of the oceans in the post K-Pg boundary interval, especially in a “microbial-loop” world where the majority of respiration took place in the surface ocean (Lowery et al., 2020), and CO_2 export was diminished. However, the lack of extinction of benthic foraminifera suggests that moderate export productivity was maintained in many but not all locations (e.g., Alegret et al., 2012; Henehan et al., 2019). The lower eukaryotic- $\text{CaCO}_3/\text{C}_{\text{org}}$ rain rate may explain the coincidence between the decrease in micrite content and the recovery of nannoplankton at the top of the micrite-rich layer.

The micrite-rich layer contains charcoal at Sites M0077 (in the crater) (Gulick et al., 2019), 738 (Kerguelen Plateau, Indian Ocean), 1210 (Shatsky Rise, Pacific Ocean) and 1262 (Walvis Ridge, South Atlantic Ocean) (Supplemental Materials Figure 3) and lies immediately above the Ir anomaly at several sites (Supplemental Materials Section 3). This suggests that micrite deposition began within years of the impact which raises a significant timing problem.

Supersaturation resulting from low eukaryotic $\text{CaCO}_3/\text{C}_{\text{org}}$ flux cannot happen within years. Simulations suggest that supersaturation (>10) requires 8.0 kyr for 50% reduction in eukaryotic $\text{CaCO}_3/\text{C}_{\text{org}}$ flux and 2.8 kyr for 75% reduction (Henehan et al., 2016). Well-preserved specimens of all crystal forms are rare so that their spatial and temporal distributions are unclear, but identifiable cyanobacterial calcite is found throughout the micrite-rich layer at distal sites (Fig. 1), with the lowermost specimens 3 cm

above the boundary at Site 1262 (approximately 5.5 kyr after the K-Pg boundary impact assuming constant sedimentation rates). At Site M0077 in the crater, proposed cyanobacterial specimens in the green marlstone unit are also up to a few millennia above the boundary (Bralower et al., *in review*). The ages of these basal specimens are consistent with the timing of supersaturation assuming low eukaryotic $\text{CaCO}_3/\text{C}_{\text{org}}$ flux (Henehan et al., 2016). Micrite in the immediate impact aftermath, i.e., in the first millennium after the impact, would either require circumstances in addition to the very low $\text{CaCO}_3/\text{C}_{\text{org}}$ flux or result from CaO reacting with CO_2 in the water column, as previously invoked to explain micrite in the proximal sites. At distal sites, CaO dispersed by the dust cloud (Artemieva and Morgan, 2020) would create, on average, a 4 cm-thick carbonate layer after carbonation, plus the consumption of CO_2 would increase saturation states leading to additional micrite precipitation. Simulations suggest that the fallout layer may have been substantially thicker at proximal sites (Artemieva and Morgan, 2020), creating even higher levels of supersaturation in these locations, and generating additional (likely abiotic) whiting material. In summary, a combination of carbonation of CaO , continued moderate export, and low $\text{CaCO}_3/\text{C}_{\text{org}}$ flux could sustain “whittings” on a global basis while promoting abiotic calcite precipitation until the calcareous nannoplankton CaCO_3 flux increased. Since this flux took several million years to recover to presumed Cretaceous levels (Alvarez et al., 2019), and dinoflagellate productivity remained high, as indicated by the abundance of cysts in shelf and deep-sea sites (Vellekoop et al., 2018; Jones et al., 2019), we conclude that conditions remained suitable for whittings well into the early Paleocene.

4.4. Ecological and evolutionary significance of the global microbial blooms

We now focus on the implications of the microbial blooms, and postulate that the thriving communities had a profound impact on organisms at higher trophic levels. The occurrence of shelled scalenohedra suggests that cyanobacteria lived inside or covering the tests of very small foraminifera, possibly dwarfed adults or juveniles. Although most foraminifera in the carbonate layer show a normal wall texture (Supplemental Materials Section 1), the abundance of shelled scalenohedral fragments suggests that these unique foraminifera were relatively common. We speculate that these foraminifera grew during whiting events with cyanobacteria encrusting their naked chambers inducing calcite precipitation. The occurrence of single scalenohedral chambers within normal foraminiferal shells (Supplemental Materials Figure 5; Pl. 5, 6) indicates that whittings could be very short-lived events, though most likely had longer durations. Thus we postulate that whiting-like blooms of microbes invaded the open ocean, along with neritic planktic foraminiferal survivors (D'Hondt and Keller, 1991), or neritic benthics evolving into planktic forms (Brinkhuis et al., 1988; Darling et al., 2009; Arenillas and Arz, 2017) in the millennia after the impact.

Globally distributed photosynthetic microbial communities were probably uniquely adapted to the extreme post-impact environments, that over the short-term were possibly dark, cold (e.g., Vellekoop et al., 2014; Brugger et al., 2017), CO_2 - (MacLeod et al., 2018) and metal- (Erickson and Dickson, 1987) rich and/or highly eutrophic (e.g., Jiang et al., 2010). Cyanobacteria today grow in cold, Arctic waters (Cota et al., 1987), under eutrophic, metal-rich conditions (Reed and Gadd, 1989), high- CO_2 concentrations (Visser et al., 2016), and under very low light levels (Knoll, 2008), and they inhabited some of the harshest environments throughout Earth history (Knoll, 2008). Some cyanobacteria and green algae are able to tolerate long intervals with low light levels (Antia and Cheng, 1970), and, along with dinoflagellates, diatoms and non-calcifying

haptophytes (Medlin et al., 2008) may well have bloomed under conditions leading to the demise of the calcifying haptophyte algae. We postulate that microbes flourished in the immediate impact aftermath, but only formed calcite skeletons when saturation became sufficiently elevated several millennia later.

Because algal and cyanobacterial blooms have the potential to tolerate high CO₂ and nutrient conditions, we postulate that the elevated microbial activity ameliorated immediate post-impact environments, making ocean surface waters habitable for other life forms. First, algal and cyanobacterial blooms could have locally or regionally removed excess nutrients that accumulated due to the absence of other primary producers (Henehan et al., 2019), or brought in because widespread fires caused denudation of the land, although microbial production would be more susceptible to remineralization in the surface ocean in a so-called “microbial loop” (Azam et al., 1983; Fenchel, 2008; Lowery et al., 2020). Second, microbial calcification led to minor net CO₂ release (Kammenaya et al., 2012), but was counteracted by growth of non-calcareous forms, causing a more significant net CO₂ draw down. There is abundant fossil and biomarker evidence for a thriving and diverse non-calcareous algal community in the impact aftermath (e.g., Brinkhuis and Zachariasse, 1988; Sepúlveda et al., 2009; Sepulveda et al., 2019; Schaefer et al., 2020). In addition, low sterane to hopane ratios suggest a flourishing non-calcareous bacterial community, likely in addition to calcareous cyanobacteria (Sepúlveda et al., 2009; Schaefer et al., 2020) although it is impossible to differentiate between primary production and organic matter degradation (possible in the “microbial loop”) for their origin. Thus, microbial blooms could have led to a net removal of CO₂ released during the impact.

The blooms enhanced the habitability of the immediate post-impact ocean, as evidenced by the sequential recovery of planktic foraminifera and nannoplankton. Foraminiferal survivors, including benthic species (e.g., Arenillas and Arz, 2017) first appeared in the lower to middle part of the carbonate layer at Site 1262 (Birch et al., 2012), and in the transitional unit at Site M0077 (Lowery et al., 2018). The first nannoplankton groups emerged in the middle of the layer, including *Braarudosphaera*, a taxon known to tolerate eutrophic coastal waters (Supplemental Materials Figure 12), and *Cervisia* (commonly named *Thoracosphaera*), a calcisphere that was cyst-forming (e.g., Hildebrand-Habel et al., 1999), an adaptive strategy for hostile surface water conditions (Anderson et al., 2008). The end of the formation of the micrite-rich layer and inferred microbial blooms is defined by the emergence of Danian coccolithophores including, at some sites, the “boom-bust” species (Bown, 2005; Jones et al., 2019). This recovery sequence suggests that cyanobacteria and non-haptophyte algae, by removing excess nutrients, and possibly CO₂ and metals, helped to condition the oceans for the recovery of calcareous phytoplankton, and were instrumental in the survival of benthic species and the recovery of the marine food web with evolution of calcifying plankton.

The extinction of over 90% of calcareous nannoplankton, dominant primary producers in the Cretaceous open ocean, may have slowed the biological pump and thus delivery of food and nutrients to the deep ocean (e.g., Kump, 1991), but probably in patterns variable by region (Alegret et al., 2012; Henehan et al., 2019). Deep sea communities including benthic foraminifera and smaller fish (Friedman, 2009; Sibert et al., 2014) were far less impacted by perturbations related to the K-Pg boundary event than surface water communities, in some cases indicating regionally higher food supply (e.g., Alegret et al., 2012), a discovery supported by elevated Ba/Ti ratios that indicate high export productivity (Hull and Norris, 2011). Replacement of calcareous nannoplankton by dinoflagellates and diatoms can explain the regionally higher export productivity and food supply (Hull et al., 2011), but both groups have poor deep-sea fossil records. Microbial carbon export, though limited by

surface ocean remineralization of sinking organic remains (Lowery et al., 2020), can explain deep-sea survival including in harsh immediate post-impact conditions, although there is another possible means of carbon export.

Our evidence suggests that microbial production may also have provided food for surface ocean biota. Planktic foraminiferal communities recovered more rapidly than calcareous nannoplankton, with earliest open-ocean assemblages dominated by Cretaceous neritic taxa (Hull et al., 2011; Lowery et al., 2018). Blooms of microbes would have served as a potential food source in the surface ocean, enabling the survival of opportunist planktic foraminifera, or their replacement by benthic forms evolving into plankton, and their full recovery before the nannoplankton (Hull et al., 2011) as well as of other grazers such as copepods (Bralower et al., in review). It is possible that these grazers and their fecal material were responsible for the majority of carbon export.

The K-Pg global microbial bloom documented here is the most extensive observed in the geological record. However, we speculate that microbial blooms following the decimation of eukaryote producers could have been key to survival and ecosystem recovery after other mass extinctions (e.g., Grice et al., 2005; Xie et al., 2005). Our novel identification of microbial fossils has potential for recognizing microbial production at other times, complementing biomarker analyses, thus the next step is to expand this investigation to earlier mass extinctions.

5. Conclusions

Abundant micrite is found in the K-Pg boundary interval at sites extending from shelf to abyssal depths characterized by depositional processes ranging from tsunami emplacement to pelagic rain. The micrite-rich layer is between a few centimeters and over seventeen meters thick. Well-preserved crystals show an array of morphologies that are indicative of a range of different origins. Simple interlocking rhombohedra resemble crystals grown from solution and are interpreted as inorganic precipitates. Close to the crater, crystals likely formed from backreaction of CaO vaporized during the impact. Crystals at numerous sites contain geologically unique, micron-sized microcrystals made of oriented agglomerates of sub-micrometer mesocrystals arranged in several regular geometries. Microcrystals show a striking resemblance to cyanobacterial calcite produced in natural environments and in culture, and the micrite-rich layer contains abundant hopanes and steranes suggesting elevated microbial production and/or degradation. Thus the layer is interpreted to represent a post-impact microbial bloom, involving bio-induced and/or bio-influenced calcite precipitation, a global whiting-like event that began within millennia of the impact and lasted up to thousands of years at some locations. The blooms thrived in supersaturated surface waters that developed in response to the abrupt extinction of the calcareous calcifiers and a decrease in the CaCO₃/C_{org} rain ratio. We hypothesize that the microbial blooms helped post impact ecosystem recovery by removing nutrients and providing a food source for higher trophic orders.

Credit authorship contribution statement

TJB conducted light and scanning microscope observations. JC and PJH helped interpret images with JW and carried out TEM analysis with CN. LRK, JVM and NA contributed interpretation of carbonate budget. DTH and JCZ analyzed and helped interpret stable isotopes and B/Ca data. SLL collected biomarker data and with KHF, KG, JC, CHH and BS helped interpret microbial ecology. AC and PJH collected XRD. HLJ and CML helped with stratigraphy at Site M0077. ET helped provide interpret global context. VV helped

identify charcoal. SG helped with overall interpretation. TJB wrote the paper and all authors helped edit.

Declaration of competing interest

There are no conflicts of interest for any of the authors of the revised manuscript

Data availability

The data that support the findings of this study are available in the PANGAEA database (<https://www.pangaea.de/>).

Acknowledgements

This research used samples and data provided by IODP Expedition 364 was jointly funded by the European Consortium for Ocean Research Drilling (ECORD) and ICDP, with contributions and logistical support from the Yucatán State Government and Universidad Nacional Autónoma de México (UNAM). Research was funded by NASA NNX12AD83G, NSF-OCE 1736951, and Post Expedition Awards from IODP to TB and KF and NSF-OCE 1737351 to CL and SG. Funding was also received from the Swedish Research Council (VR grant 2015-4264 to VV. KG and BS were supported by an Australian Research Council (ARC - DP180100982) and Australian and New Zealand legacy IODP funding (364), 2016-2018. JM received NERC funding (NE/P005217/1). We thank Holger Kuhlmann, Lallan Gupta, Chad Broyles, and Phil Rumford for help with sampling ocean cores, Julie Anderson and Wes Auker for help with the SEM, Jenn Grey for assistance with TEM, Max Wetherington for assistance with Raman, and Professor Bin Lian for sharing published photographs of cyanobacteria in Fig. 2. We acknowledge discussions with Paul Bown, Michael Henehan, Paul Pearson, Howie Spero and Jeremy Young. We thank Michael Henehan for extremely helpful feedback on an earlier version of this manuscript as well as comments by two other reviewers. We thank Aileen McNamee and Carly Gazze for technical help. Land section samples were generously supplied by Hermann Bermudez, Eduardo Kousoutkos, Julio Sepúlveda, and Laia Alegret; samples from Site 384 were lent by Hans Thierstein, and picked foraminifera from Site 1049 were supplied by Brian Huber. This is UTIG Contribution #3664 and Center for Planetary Systems Habitability #0009.

Appendix A. Supplementary material

Supplementary material related to this article can be found online at <https://doi.org/10.1016/j.epsl.2020.116476>.

References

- Agrinier, P., Deutsch, A., Schärer, U., Martinez, I., 2001. Fast back-reactions of shock-released CO₂ from carbonates: an experimental approach. *Geochim. Cosmochim. Acta* 65, 2615–2632.
- Alegret, L., Thomas, E., 2013. Benthic foraminifera across the Cretaceous/Paleogene boundary in the Southern Ocean (ODP Site 690): diversity, food and carbonate saturation. *Mar. Micropaleontol.* 105, 40–51.
- Alegret, L., Thomas, E., Lohmann, K.C., 2012. End-Cretaceous marine mass extinction not caused by productivity collapse. *Proc. Natl. Acad. Sci.* 109, 728–732.
- Alroy, J., 2008. Dynamics of origination and extinction in the marine fossil record. *Proc. Natl. Acad. Sci.* 105, 11536–11542.
- Alvarez, S.A., Gibbs, S.J., Bown, P.R., Kim, H., Sheward, R.M., Ridgwell, A., 2019. Diversity decoupled from ecosystem function and resilience during mass extinction recovery. *Nature* 574, 242–245.
- Anbu, P., Kang, C.H., Shin, Y.J., So, J.S., 2016. Formations of calcium carbonate minerals by bacteria and its multiple applications. *SpringerPlus* 5, 250.
- Anderson, D.M., Burkholder, J.M., Cochlan, W.P., Glibert, P.M., Gobler, C.J., Heil, C.A., Kudela, R.M., Parsons, M.L., Rensel, J.J., Townsend, D.W., 2008. Harmful algal blooms and eutrophication: examining linkages from selected coastal regions of the United States. *Harmful Algae* 8, 39–53.
- Antia, N., Cheng, J., 1970. The survival of axenic cultures of marine planktonic algae from prolonged exposure to darkness at 20 °C. *Phycologia* 9, 179–183.
- Arenillas, I., Arz, J.A., 2017. Benthic origin and earliest evolution of the first planktonic foraminifera after the Cretaceous/Palaeogene boundary mass extinction. *Hist. Biol.* 29, 25–42.
- Arp, G., Thiel, V., Reimer, A., Michaelis, W., Reitner, J., 1999. Biofilm exopolymers control microbialite formation at thermal springs discharging into the alkaline Pyramid Lake, Nevada, USA. *Sediment. Geol.* 126, 159–176.
- Artemieva, N., Morgan, J., 2020. Global K-Pg layer deposited from a dust cloud. *Geophys. Res. Lett.*, 2019GL086562. <https://doi.org/10.1029/2019GL086562>.
- Azam, F., Fenchel, T., Field, J.G., Gray, J., Meyer-Reil, L., Thingstad, F., 1983. The ecological role of water-column microbes in the sea. *Mar. Ecol. Prog. Ser.* 257–263.
- Bang, S.S., Galinat, J.K., Ramakrishnan, V., 2001. Calcite precipitation induced by polyurethane-immobilized *Bacillus pasteurii*. *Enzyme Microb. Technol.* 28, 404–409.
- Benzerara, K., Miot, J., Morin, G., Ona-Nguema, G., Skouri-Panet, F., Ferard, C., 2011. Significance, mechanisms and environmental implications of microbial biomineralization. *C. R. Geosci.* 343, 160–167.
- Birch, H.S., Coxall, H.K., Pearson, P.N., 2012. Evolutionary ecology of Early Paleocene planktonic foraminifera: size, depth habitat and symbiosis. *Paleobiology* 38, 374–390.
- Bobrovskiy, I., Hope, J.M., Brocks, J.J., 2019. Analysis of biomarkers from ediacaran fossils: bringing together palaeontology and organic geochemistry. In: 29th International Meeting on Organic Geochemistry.
- Boudreau, B.P., Middelburg, J.J., Luo, Y., 2018. The role of calcification in carbonate compensation. *Nat. Geosci.* 11, 894–900.
- Bown, P., 2005. Selective calcareous nannoplankton survivorship at the Cretaceous-Tertiary boundary. *Geology* 33, 653.
- Bown, P.R., Lees, J.A., Young, J.R., 2004. *Calcareous Nannoplankton Evolution and Diversity Through Time, Coccolithophores*. Springer, pp. 481–508.
- Bralower, T.J., Cosmidis, Fantle M. J., Lowery, C., Passey, B., Gulick, S., Morgan, J., Vajda, V., Whalen, M., Wittmann, A., Artemieva, N., Farley, K., Goderis, S., Hajek, E., Heaney, P., Kring, D., Lyons, S., Rasmussen, C., Sibert, E., Tovar, Gordon Turner-Walker G. F., Zachos, J., Carte, J., Chen, S., Cockell, C., Coolen, M., Freeman, K., Garber, J., Gray, J., Gonzales, M., Grice, K., Jones, H., Schaefer, B., Smit, J., Tikoo, S., The habitat of the nascent Chicxulub crater, AGU Advances, in review.
- Bralower, T.J., Paull, C.K., Leckie, R.M., 1998. The Cretaceous-Tertiary boundary cocktail: Chicxulub impact triggers margin collapse and extensive sediment gravity flows. *Geology* 26, 331–334.
- Bralower, T.J., Premoli Silva, I., Malone, M., 2002. New evidence for abrupt climate change in the Cretaceous and Paleogene: an ocean drilling program expedition to Shatsky Rise, northwest Pacific. *GSA Today* 12, 4–10.
- Bravais, A., 1866. *Etudes Cristallographiques*. Gauthier-Villars, Paris, France. Surface Energy Chapter 5.
- Brinkhuis, H., Zachariasse, W.J., 1988. Dinoflagellate cysts, sea level changes and planktonic foraminifers across the Cretaceous-Tertiary boundary at El Haria, northwest Tunisia. *Mar. Micropaleontol.* 13, 153–191.
- Brown, R.E., Anderson, L.D., Thomas, E., Zachos, J.C., 2011. A core-top calibration of Ba/Ca in the benthic foraminifers Nuttallides umbonifera and Oridorsalis umboatus: a proxy for Cenozoic bottom water carbonate saturation. *Earth Planet. Sci. Lett.* 310, 360–368.
- Brugger, J., Feulner, G., Petri, S., 2017. Baby, it's cold outside: climate model simulations of the effects of the asteroid impact at the end of the Cretaceous. *Geophys. Res. Lett.* 44, 419–427.
- Caldeira, K., Rampino, M.R., 1993. Aftermath of the end-Cretaceous mass extinction: possible biogeochemical stabilization of the carbon cycle and climate. *Paleoceanography* 8, 515–525.
- Cao, C., Jiang, J., Sun, H., Huang, Y., Tao, F., Lian, B., 2016. Carbonate mineral formation under the influence of limestone-colonizing actinobacteria: morphology and polymorphism. *Front. Microbiol.* 7, 366.
- Casella, L.A., Griesshaber, E., Roda, M.S., Ziegler, A., Mavromatis, V., Henkel, D., Laudien, J., Häussermann, V., Neuser, R., Angiolini, L., 2018. Micro- and nanostructures reflect the degree of diagenetic alteration in modern and fossil brachiopod shell calcite: a multi-analytical screening approach (CL, FE-SEM, AFM, EBSD). *Paleogeogr. Palaeoclimatol. Palaeoecol.* 502, 13–30.
- Cizer, Ö., Rodriguez-Navarro, C., Ruiz-Agudo, E., Elsen, J., Van Gemert, D., Van Balen, K., 2012. Phase and morphology evolution of calcium carbonate precipitated by carbonation of hydrated lime. *J. Mater. Sci.* 47, 6151–6165.
- Colfen, H., Antonietti, M., 2005. Mesocrystals: inorganic superstructures made by highly parallel crystallization and controlled alignment. *Angew. Chem., Int. Ed. Engl.* 44, 5576–5591.
- Coshell, E., Rosen, M., McNamara, K., 1998. Hydromagnesite replacement of biomineralized aragonite in a new location of Holocene stromatolites, Lake Walyungup, Western Australia. *Sedimentology* 45, 1005–1018.
- Cota, G., Prinsenberg, S., Bennett, E., Loder, J., Lewis, M., Anning, J., Watson, N., Harris, L., 1987. Nutrient fluxes during extended blooms of Arctic ice algae. *J. Geophys. Res., Oceans* 92, 1951–1962.
- Couradeau, E., Benzerara, K., Gérard, E., Estève, I., Moreira, D., Tavares, R., López-García, P., 2013. Cyanobacterial calcification in modern microbialites at the sub-micrometer scale. *Biogeosciences* 10, 5255–5266.

- Cuif, J.-P., Dauphin, Y., 2005. The two-step mode of growth in the scleractinian coral skeletons from the micrometre to the overall scale. *J. Struct. Biol.* 150, 319–331.
- Darling, K.F., Thomas, E., Kasemann, S.A., Sears, H.A., Smart, C.W., Wade, C.M., 2009. Surviving mass extinction by bridging the benthic/planktic divide. *Proc. Natl. Acad. Sci.* 106, 12629–12633.
- De Yoreo, J.J., Gilbert, P.U., Sommerdijk, N.A., Penn, R.L., Whitelam, S., Joester, D., Zhang, H., Rimer, J.D., Navrotzky, A., Banfield, J.F., 2015. Crystallization by particle attachment in synthetic, biogenic, and geologic environments. *Science* 349, aaa6760.
- D'Hondt, S., 2005. Consequences of the Cretaceous/Paleogene mass extinction for marine ecosystems. *Annu. Rev. Ecol. Evol. Syst.* 36, 295–317.
- D'Hondt, S., Keller, G., 1991. Some patterns of planktic foraminiferal assemblage turnover at the Cretaceous-Tertiary boundary. *Mar. Micropaleontol.* 17, 77–118.
- D'Hondt, S., Pilson, M.E., Sigurdsson, H., Hanson, A.K., Carey, S., 1994. Surface-water acidification and extinction at the Cretaceous-Tertiary boundary. *Geology* 22, 983–986.
- Dupraz, C., Visscher, P.T., 2005. Microbial lithification in marine stromatolites and hypersaline mats. *Trends Microbiol.* 13, 429–438.
- Dupraz, C., Reid, R.P., Braissant, O., Decho, A.W., Norman, R.S., Visscher, P.T., 2009. Processes of carbonate precipitation in modern microbial mats. *Earth-Sci. Rev.* 96, 141–162.
- Erickson, D.J., Dickson, S.M., 1987. Global trace-element biogeochemistry at the K/T boundary: oceanic and biotic response to a hypothetical meteorite impact. *Geology* 15, 1014–1017.
- Fabricius, I.L., 2007. Chalk: composition, diagenesis and physical properties. *Bull. Geol. Soc. Den.* 55, 97–128.
- Fenchel, T., 2008. The microbial loop—25 years later. *J. Exp. Mar. Biol. Ecol.* 366, 99–103.
- Friedman, M., 2009. Ecomorphological selectivity among marine teleost fishes during the end-Cretaceous extinction. *Proc. Natl. Acad. Sci. USA* 0808468106.
- Gilbert, P.U., Porter, S.M., Sun, C.-Y., Xiao, S., Gibson, B.M., Shenkar, N., Knoll, A.H., 2019. Biomineralization by particle attachment in early animals. *Proc. Natl. Acad. Sci.* 116, 17659–17665.
- Goderis, S., Sato, H., et al., 2019. The final settling of meteoritic matter on the peak-ring of the Chicxulub impact structure at Site M0077A of IODP-ICDP expedition 364. In: Large Meteorite Impacts and Planetary Evolution VI.
- Goetz, A.J., Griesshaber, E., Abel, R., Fehr, T., Ruthensteiner, B., Schmahl, W.W., 2014. Tailored order: the mesocrystalline nature of sea urchin teeth. *Acta Biomater.* 10, 3885–3898.
- Golubic, S., Le Campion-Alsumard, T., Campbell, S.E., 1999. Diversity of marine cyanobacteria. *Bulletin-Institut Oceanographique Monaco-Numeros Special-*, 53–76.
- Greer, H.F., Zhou, W., Guo, L., 2017. Reversed crystal growth of calcite in naturally occurring travertine crust. *Crystals* 7, 36.
- Grice, K., Cao, C., Love, G.D., Böttcher, M.E., Twitchett, R.J., Grosjean, E., Summons, R.E., Turgeon, S.C., Dunning, W., Jin, Y., 2005. Photic zone euxinia during the Permian-Triassic superoxic event. *Science* 307, 706–709.
- Gulick, S., Bralower, T.J., Ormö, J., Hall, B., Grice, K., Schaefer, B., Lyons, S., Freeman, K., Morgan, J., Artemieva, N., Kaskes, P., de Graaff, S., Whalen, M., Goto, K., Smit, J., et al., 2019. The first day of the Cenozoic. *Proc. Natl. Acad. Sci.* 113, 19342–19351.
- Han, Z., Meng, R., Yan, H., Zhao, H., Han, M., Zhao, Y., Sun, B., Sun, Y., Wang, J., Zhuang, D., 2017. Calcium carbonate precipitation by *Synechocystis* sp. PCC6803 at different Mg/Ca molar ratios under the laboratory condition. *Carbonates Evaporites* 32, 561–575.
- Heberling, F., Trainor, T.P., Lützenkirchen, J., Eng, P., Denecke, M.A., Bosbach, D., 2011. Structure and reactivity of the calcite–water interface. *J. Colloid Interface Sci.* 354, 843–857.
- Henehan, M.J., Hull, P.M., Penman, D.E., Rae, J.W., Schmidt, D.N., 2016. Biogeochemical significance of pelagic ecosystem function: an end-Cretaceous case study. *Philos. Trans. R. Soc. Lond. B, Biol. Sci.* 371.
- Henehan, M.J., Ridgwell, A., Thomas, E., Zhang, S., Alegret, L., Schmidt, D.N., Rae, J.W., Witts, J.D., Landman, N.H., Greene, S.E., 2019. Rapid ocean acidification and protracted Earth system recovery followed the end-Cretaceous Chicxulub impact. *Proc. Natl. Acad. Sci.* 116, 22500–22504.
- Hildebrand, A.R., Penfield, G.T., Kring, D.A., Pilkington, M., Camargo, A., Jacobsen, S.B., Boynton, W.V., 1991. Chicxulub crater: a possible Cretaceous/Tertiary boundary impact crater on the Yucatan Peninsula, Mexico. *Geology* 19, 867–871.
- Hildebrand-Habel, T., Willems, H., Versteegh, G., 1999. Variations in calcareous dinoflagellate associations from the Maastrichtian to middle Eocene of the western South Atlantic Ocean (São Paulo Plateau, DSDP Leg 39, Site 356). *Rev. Palaeobot. Palynol.* 106, 57–87.
- Huber, B., 1991. Maestrichtian planktonic foraminifer biostratigraphy and the Cretaceous/Tertiary boundary at Hole 738C (Kerguelen Plateau, southern Indian Ocean). In: Proceedings of the Ocean Drilling Program, Scientific Results, pp. 451–462.
- Hull, P.M., Norris, R.D., 2011. Diverse patterns of ocean export productivity change across the Cretaceous-Paleogene boundary: new insights from biogenic barium. *Paleoceanography* 26.
- Hull, P.M., Norris, R.D., Bralower, T.J., Schueth, J.D., 2011. A role for chance in marine recovery from the end-Cretaceous extinction. *Nat. Geosci.* 4, 856–860.
- Hull, P.M., Bornemann, A., Penman, D.E., Henehan, M.J., Norris, R.D., Wilson, P.A., Blum, P., Alegret, L., Batenburg, S.J., Bown, P.R., 2020. On impact and volcanism across the Cretaceous-Paleogene boundary. *Science* 367, 266–272.
- Ishikawa, T., Nakamura, E., 1993. Boron isotope systematics of marine sediments. *Earth Planet. Sci. Lett.* 117, 567–580.
- Jablonski, D., 1986. Background and mass extinctions: the alternation of macroevolutionary regimes. *Science* 231, 129–134.
- Jiang, S., Bralower, T.J., Patzkowsky, M.E., Kump, L.R., Schueth, J.D., 2010. Geographic controls on nannoplankton extinction across the Cretaceous/Paleogene boundary. *Nat. Geosci.* 3, 280–285.
- Jones, B., 2017a. Review of aragonite and calcite crystal morphogenesis in thermal spring systems. *Sediment. Geol.* 354, 9–23.
- Jones, B., 2017b. Review of calcium carbonate polymorph precipitation in spring systems. *Sediment. Geol.* 353, 64–75.
- Jones, B., Renaut, R.W., 2017. Modern travertine precipitation at Lýsuhóll hot springs, Snæfellsnes, Iceland: implications for calcite crystal growth. *J. Sediment. Res.* 87, 1121–1142.
- Jones, H.L., Lowery, C.M., Bralower, T.J., 2019. Calcareous nannoplankton “boom-bust” successions in the Cretaceous-Paleogene (K-Pg) impact crater suggests ecological experimentation at “ground zero”. *Geology* 47, 753–756.
- Kamennaya, N.A., Ajo-Franklin, C.M., Northen, T., Jansson, C., 2012. Cyanobacteria as biocatalysts for carbonate mineralization. *Minerals* 2, 338–364.
- Katz, M.E., Finkel, Z.V., Grzebyk, D., Knoll, A.H., Falkowski, P.G., 2004. Evolutionary trajectories and biogeochemical impacts of marine eukaryotic phytoplankton. *Annu. Rev. Ecol. Evol. Syst.* 35, 523–556.
- Knoll, A.H., 2008. Cyanobacteria and Earth history. In: *The Cyanobacteria: Molecular Biology, Genomics and Evolution*. 484.
- Knoll, A.H., Follows, M.J., 2016. A bottom-up perspective on ecosystem change in Mesozoic oceans. *Proc. R. Soc. Lond. B, Biol. Sci.* 283, 20161755.
- Kring, D.A., 2007. The Chicxulub impact event and its environmental consequences at the Cretaceous-Tertiary boundary. *Palaeogeogr. Palaeoclimatol. Palaeoecol.* 255, 4–21.
- Kring, D.A., Durda, D.D., 2002. Trajectories and distribution of material ejected from the Chicxulub impact crater: implications for postimpact wildfires. *J. Geophys. Res., Planets* 107, 6–1–6–22.
- Kump, L.R., 1991. Interpreting carbon-isotope excursions: *Strangelove* oceans. *Geology* 19, 299–302.
- Lemarchand, D., Wasserburg, G., Papanastassiou, D., 2004. Rate-controlled calcium isotope fractionation in synthetic calcite. *Geochim. Cosmochim. Acta* 68, 4665–4678.
- Lowery, C.M., Bralower, T.J., Owens, J.D., Rodriguez-Tovar, F.J., Jones, H., Smit, J., Whalen, M.T., Claeys, P., Farley, K., Gulick, S.P.S., Morgan, J.V., Green, S., Chenot, E., Christeson, G.L., Cockell, C.S., Coolen, M.J.L., Ferrière, L., Gebhardt, C., Goto, K., Kring, D.A., Lofi, J., Ocampo-Torres, R., Perez-Cruz, L., Pickersgill, A.E., Poelchau, M.H., Rae, A.S.P., Rasmussen, C., Rebollo-Vieyra, M., Riller, U., Sato, H., Tikoo, S.M., Tomioka, N., Urutia-Fucugauchi, J., Vellekoop, J., Wittmann, A., Xiao, L., Yamaguchi, K.E., Zylberman, W., 2018. Rapid recovery of life at ground zero of the end-Cretaceous mass extinction. *Nature* 558, 288–291.
- Lowery, C.M., Jones, H.J., Bralower, T.J., Perez Cruz, L., Gebhardt, C., Whalen, M.T., Chenot, E., Jan Smit, J., Purkey Phillips, M., Choumiline, K., Arenillas, I., Arz, J.A., Garcia, F., Ferrand, M., Gulick, S.P.S., 2020. Early Paleocene paleoceanography and export productivity in the Chicxulub Crater. *Paleoceanogr. Paleoclimatol.*
- Lyons, S.L., Karp, A.T., Bralower, T.J., Grice, K., Schaefer, B., Gulick, S.P.S., Morgan, J., Freeman, K.H., 2019. Organic matter from the Chicxulub crater exacerbated the K-Pg impact winter, *PNAS*, in press
- MacLeod, K., Quinton, P., Sepúlveda, J., Negra, M., 2018. Postimpact earliest Paleogene warming shown by fish debris oxygen isotopes (El Kef, Tunisia). *Science* 360, 1467–1469.
- MacLeod, K.G., Whitney, D.L., Huber, B.T., Koeberl, C., 2007. Impact and extinction in remarkably complete Cretaceous-Tertiary boundary sections from Demerara Rise, tropical western North Atlantic. *Geol. Soc. Am. Bull.* 119, 101–115.
- Magill, C.R., Denis, E.H., Freeman, K.H., 2015. Rapid sequential separation of sedimentary lipid biomarkers via selective accelerated solvent extraction. *Org. Geochem.* 88, 29–34.
- Medlin, L., Sáez, A.G., Young, J.R., 2008. A molecular clock for coccolithophores and implications for selectivity of phytoplankton extinctions across the K/T boundary. *Mar. Micropaleontol.* 67, 69–86.
- Meldrum, F.C., Hyde, S.T., 2001. Morphological influence of magnesium and organic additives on the precipitation of calcite. *J. Cryst. Growth* 231, 544–558.
- Minoletti, F., de Rafelis, M., Renard, M., Gardin, S., Young, J., 2005. Changes in the pelagic fine fraction carbonate sedimentation during the Cretaceous–Paleocene transition: contribution of the separation technique to the study of Bidart section. *Palaeogeogr. Palaeoclimatol. Palaeoecol.* 216, 119–137.
- Morgan, J., Gulick, S., Bralower, T., Chenot, E., Christeson, G., Claeys, P., Cockell, C., Collins, G.S., Coolen, M.J., Ferrière, L., 2016. The formation of peak rings in large impact craters. *Science* 354, 878–882.
- Obst, M., Wehrli, B., Dittrich, M., 2009. CaCO₃ nucleation by cyanobacteria: laboratory evidence for a passive, surface-induced mechanism. *Geobiology* 7, 324–347.
- Pacton, M., Hunger, G., Martinuzzi, V., Cusminsky, G., Burdin, B., Barnett, K., Vasconcelos, C., Ariztegui, D., 2015. Organomineralization processes in freshwater stromatolites: a living example from eastern Patagonia. *Depos. Rec.* 1, 130–146.

- Peng, X., Jones, B., 2013. Patterns of biomediated CaCO₃ crystal bushes in hot spring deposits. *Sediment. Geol.* 294, 105–117.
- Pérez-Huerta, A., Coronado, I., Hegna, T.A., 2018. Understanding biomineralization in the fossil record. *Earth-Sci. Rev.* 179, 95–122.
- Perry, R.S., McLoughlin, N., Lynne, B.Y., Sephton, M.A., Oliver, J.D., Perry, C.C., Campbell, K., Engel, M.H., Farmer, J.D., Brasier, M.D., 2007. Defining biominerals and organominerals: direct and indirect indicators of life. *Sediment. Geol.* 201, 157–179.
- Reed, R., Gadd, G., 1989. Metal tolerance in eukaryotic and prokaryotic algae. In: Heavy Metal Tolerance in Plants: Evolutionary Aspects, pp. 105–118.
- Ricci, J.N., Coleman, M.L., Welander, P.V., Sessions, A.L., Summons, R.E., Spear, J.R., Newman, D.K., 2014. Diverse capacity for 2-methylhopanoid production correlates with a specific ecological niche. *ISME J.* 8, 675.
- Robbins, L., Blackwelder, P., 1992. Biochemical and ultrastructural evidence for the origin of whittings: a biologically induced calcium carbonate precipitation mechanism. *Geology* 20, 464–468.
- Röhl, U., Ogg, J.G., Geib, T.L., Wefer, G., 2001. Astronomical Calibration of the Danian Time Scale. Special Publications, vol. 183. Geological Society, London, pp. 163–183.
- Schaefer, B., Grice, K., Coolen, M.J.L., Summons, R.E., Cui, X., Bauersachs, T., Schwark, L., Böttcher, M.E., Bralower, T.J., Lyons, S.L., Freeman, K.H., Cockell, C.S., Gulick, S.P.S., Morgan, J.V., Whalen, M.T., Lowery, C.M., Vajda, V., 2020. Microbial life in the nascent Chicxulub crater. *Geology* 48 (4), 328–332.
- Scholle, P.A., 1977. Chalk diagenesis and its relation to petroleum exploration: oil from chalks, a modern miracle? *Am. Assoc. Pet. Geol. Bull.* 61, 982–1009.
- Schopf, J.W., Kudryavtsev, A.B., Sugitani, K., Walter, M.R., 2010. Precambrian microbe-like pseudofossils: a promising solution to the problem. *Precambrian Res.* 179, 191–205.
- Schulte, P., Deutsch, A., Salge, T., Berndt, J., Kontny, A., MacLeod, K.G., Neuser, R.D., Krumm, S., 2009. A dual-layer Chicxulub ejecta sequence with shocked carbonates from the Cretaceous-Paleogene (K-Pg) boundary, Demerara Rise, western Atlantic. *Geochim. Cosmochim. Acta* 73, 1180–1204.
- Schulte, P., Alegret, L., Arenillas, I., Arz, J.A., Barton, P.J., Bown, P.R., Bralower, T.J., Christeson, G.L., Claeys, P., Cockell, C.S., Collins, G.S., Deutsch, A., Goldin, T.J., Goto, K., Grajales-Nishimura, J.M., Grieve, R.A., Gulick, S.P., Johnson, K.R., Kiessling, W., Koebler, C., Krings, D.A., MacLeod, K.G., Matsui, T., Melosh, J., Montanari, A., Morgan, J.V., Neal, C.R., Nichols, D.J., Norris, R.D., Pierazzo, E., Ravizza, G., Rebollo-Vieyra, M., Reimold, W.U., Robin, E., Salge, T., Speijer, R.P., Sweet, A.R., Urrutia-Fucugauchi, J., Vajda, V., Whalen, M.T., Willumsen, P.S., 2010. The Chicxulub asteroid impact and mass extinction at the Cretaceous-Paleogene boundary. *Science* 327, 1214–1218.
- Schultze-Lam, S., Beveridge, T.J., Des Marais, D.J., 1997. Whiting events: biogenic origin due to the photosynthetic activity of cyanobacterial picoplankton. *Limnol. Oceanogr.* 42, 133–141.
- Sepkoski, J.J., 1996. Patterns of Phanerozoic extinction: a perspective from global data bases. In: Global Events and Event Stratigraphy in the Phanerozoic. Springer, pp. 35–51.
- Sepulveda, J., Wendler, J.E., Summons, R.E., Hinrichs, K.-U., 2009. Rapid resurgence of marine productivity after the Cretaceous-Paleogene mass extinction. *Science* 326, 129–132.
- Sepulveda, J., Alegret, L., Thomas, E., Haddad, E., Cao, C., Summons, R.E., 2019. Stable isotope constraints on marine productivity across the Cretaceous-Paleogene mass extinction. *Paleoceanogr. Paleoclimatol.* 34, 1195–1217.
- Seto, J., Ma, Y., Davis, S.A., Meldrum, F., Gourrier, A., Kim, Y.-Y., Schilde, U., Sztucki, M., Burghammer, M., Maltsev, S., 2012. Structure-property relationships of a biological mesocrystal in the adult sea urchin spine. *Proc. Natl. Acad. Sci.* 109, 3699–3704.
- Sibert, E.C., Hull, P.M., Norris, R.D., 2014. Resilience of Pacific pelagic fish across the Cretaceous/Paleogene mass extinction. *Nat. Geosci.* 7, 667.
- Thierstein, H.R., 1982. Terminal Cretaceous Plankton Extinctions: A Critical Assessment. In: Geological Implications of Impacts of Large Asteroids and Comets on the Earth. Geological Society of America, pp. 385–399. Special Paper.
- Thierstein, H.R., Asaro, F., Ehrmann, W.U., Huber, B., Michel, H., Sakai, H., Schmitz, B., 1991. The Cretaceous/Tertiary boundary at Site 738 Southern Kerguelen Plateau. In: Proc. ODP, Sci. Results, Vol. 119.
- Thompson, J.B., 2000. Microbial Whittings, Microbial Sediments. Springer, pp. 250–260.
- Uchikawa, J., Penman, D.E., Zachos, J.C., Zeebe, R.E., 2015. Experimental evidence for kinetic effects on B/Ca in synthetic calcite: implications for potential B(OH)₄⁻ and B(OH)₃ incorporation. *Geochim. Cosmochim. Acta* 150, 171–191.
- Vellekoop, J., Sluijs, A., Smit, J., Schouten, S., Weijers, J.W., Damsté, J.S.S., Brinkhuis, H., 2014. Rapid short-term cooling following the Chicxulub impact at the Cretaceous-Paleogene boundary. *Proc. Natl. Acad. Sci. USA* 111, 7537–7541.
- Vellekoop, J., Woelders, L., van Helmond, N.A., Galeotti, S., Smit, J., Slomp, C.P., Brinkhuis, H., Claeys, P., Speijer, R.P., 2018. Shelf hypoxia in response to global warming after the Cretaceous-Paleogene boundary impact. *Geology* 46, 683–686.
- Visser, P.M., Verspagen, J.M., Sandrini, G., Stal, L.J., Matthijs, H.C., Davis, T.W., Paerl, H.W., Huisman, J., 2016. How rising CO₂ and global warming may stimulate harmful cyanobacterial blooms. *Harmful Algae* 54, 145–159.
- Weiner, S., Dove, P.M., 2003. An overview of biomineralization processes and the problem of the vital effect. *Rev. Mineral. Geochem.* 54, 1–29.
- Westerhold, T., Röhl, U., Raffi, I., Fornaciari, E., Monechi, S., Reale, V., Bowles, J., Evans, H.F., 2008. Astronomical calibration of the Paleocene time. *Palaeogeogr. Palaeoclimatol. Palaeoecol.* 257, 377–403.
- Xie, S., Pancost, R.D., Yin, H., Wang, H., Evershed, R.P., 2005. Two episodes of microbial change coupled with Permo/Triassic faunal mass extinction. *Nature* 434 (7032), 494.
- Yancey, T.E., Guillemette, R.N., 2008. Carbonate accretionary lapilli in distal deposits of the Chicxulub impact event. *Geol. Soc. Am. Bull.* 120, 1105–1118.
- Yang, W., Ahrens, T.J., 1998. Shock vaporization of anhydrite and global effects of the K/T bolide. *Earth Planet. Sci. Lett.* 156, 125–140.
- Yu, J., Elderfield, H., Hönnisch, B., 2007. B/Ca in planktonic foraminifera as a proxy for surface seawater pH. *Paleoceanogr. Paleoclimatol.* 22, PA2202.
- Zachos, J., Arthur, M., 1986. Paleoceanography of the Cretaceous/Tertiary boundary event: inferences from stable isotopic and other data. *Palaeogeogr. Palaeoclimatol.* 1, 5–26.



Timothy Bralower is a Professor in the Department of Geosciences at Penn State University. He received his BA from Oxford and his PhD from Scripps Institution of Oceanography. Bralower is a micropaleontologist and marine geologist with interests in mass extinction and abrupt climate change. He was co-chief scientist on Ocean Drilling Program Leg 198 when the K-Pg micrite layer was first recognized and a shipboard scientist on the joint International Ocean

Drilling Program-International Continental Drilling Program (IODP-ICDP) Expedition 364 to drill the Chicxulub crater. Bralower is heavily involved in online sustainability education through the Penn State World Campus.



Julie Cosmidis received her PhD in Geochemistry from the Institut de Physique du Globe de Paris and University Paris 7 in 2013. She worked as a postdoctoral Research Associate at the University of Colorado in Boulder, and is now an Assistant Professor in Geosciences at Penn State University. Her work focuses on microbial biomineralization and microbial biosignatures.



Peter Heaney is a Professor in the Department of Geosciences at Penn State University with a focus on environmental mineralogy. His research group explores the ability of soil minerals to remove toxic metals from surface and ground waters, using a range of X-ray and electron probes that offer an atomic-scale view of metal sequestration. In addition, he investigates nanocrystal growth, dissolution, and transformation in hydrous environments.



Lee Kump is Dean of the College of Earth and Mineral Sciences and a biogeochemist in the Department of Geosciences at Penn State. For the last several years, research in his group has focused on unraveling the drivers and consequences of abrupt climate and biotic change in Earth history, using a variety of approaches including field work in modern and ancient settings, measurement of isotope and other proxy records, and interpretation of those records using numerical models of various complexities, time-series analysis, and data assimilation.



Joanna Morgan is a Professor at the Department of Earth Science and Engineering at Imperial College London, UK. She is a geophysicist who specializes in inversion of the full seismic wavefield to recover high-resolution images of the subsurface. She has been working on Chicxulub for over 20 years, used seismic data to determine its size and morphology, worked on crater formation and ejection of material around the globe, and was one of the co-chief scientists on IODP-ICDP Expedition 364 that drilled into the crater.



Dustin Harper received his Bachelor's and Master's degrees from the University of California San Diego and his PhD from the University of California Santa Cruz. His research utilizes geochemical proxies in carbonates to reconstruct changes in the carbon cycle, climate, the hydrologic cycle and ocean chemistry during warm intervals of the Cretaceous and Paleogene on long (Myrs) and short (kyrs) timescales. Currently, he is a postdoctoral researcher at the University of Kansas where he has expanded his marine-focused work to terrestrial environments.



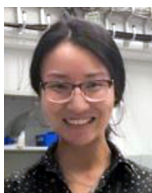
Shelby Lyons received her Bachelor's degree in Chemistry from Haverford College and her PhD in Geosciences at Penn State University. She is an organic geochemist, and her primary research focus is on the link between the organic carbon cycle and climatic changes in Earth's past. Her work develops new ways to identify and assess the impacts of ancient, recycled organic matter in marine sediments. She is currently a geoscientist at ExxonMobil.



James C. Zachos, Professor and Chair of the Earth and Planetary Sciences Department at the University of California, Santa Cruz, received his PhD in 1988 from the Graduate School of Oceanography, University of Rhode Island. His research explores aspects of ocean, climate, and carbon cycle dynamics over the Cretaceous and Cenozoic with a specific focus on periods of rapid and extreme climate change, and issues ranging from the causes of extreme greenhouse warming and ocean acidification to the onset of Antarctic glaciation.



Natalia Artemieva received her Master's and PhD degrees in Moscow, Russia. She is currently a senior scientist at the Planetary Science Institute in Tucson, Arizona and a frequent visiting scientist at the Naturkunde Museum in Berlin. She uses computer simulations to study high-velocity impacts including interaction of asteroids with the atmosphere, crater formation and ejecta deposition.



Si Athena Chen is currently a PhD Candidate in Mineralogy and Environmental Geochemistry in the Department of Geosciences, Penn State University. She studies mineral phase transformation as an indicator of environmental changes, particularly the transformation of iron (hydr)oxides. Chen specializes in mineralogical, nanostructural, and geochemical characterization of minerals using X-ray Diffraction, Electron Microscopes, and various Spectroscopies.



Research Professor Sean Gulick, his students, and colleagues are working on tectonic and climate interactions, geohazards and continental margin evolution, and the geologic processes and environmental effects of meteor impacts. In 2016, he served as Co-Chief Scientist on the joint IODP-ICDP Expedition 364: Drilling the K-Pg Chicxulub impact crater, and is the Co-Director of the Center for Planetary Systems Evolution at the University of Texas at Austin.



Christopher House received his Bachelor's degree in Biochemistry and Cell Biology from the University of California, San Diego. He then received his PhD in Geology from the University of California, Los Angeles. He is a Professor of Geosciences at Penn State University, where he is the Director for the Astrobiology Research Center, and the Director of the Pennsylvania Space Grant Consortium. His research is on microbial geochemistry, and signatures of microbial life.



Heather Jones received her integrated Master's degree in Geology from the University of Southampton (UK) where she first discovered her love for calcareous nannoplankton. She recently received her PhD in Geosciences from Penn State University, which was partly funded by a Schlanger Ocean Drilling Fellowship. Heather is heavily involved with the International Ocean Discovery Program (IODP), having sailed as a nannofossil biostratigrapher on Expedition 364 (Chicxulub impact crater), and more recently as a physical properties specialist on Expedition 378 (South Pacific Paleogene Climate). She is broadly interested in the ecological and evolutionary response of calcareous nannoplankton to extreme environmental perturbation throughout the geologic record.



Jens E. Wendler received his Master's degree in Geosciences from TU Mining Academy Freiberg, Germany, and a PhD from Bremen University, Germany.

He held research positions at Bremen University and at the Smithsonian Institution, Washington D.C. His research is focused on carbonate biomimicry, marine micropaleontology and paleoclimatology, and one of his main achievements was the discovery of new biomimicry styles in calcareous dinoflagellates. He currently is a researcher and lecturer in carbonate petrography and paleoclimatology at Friedrich-Schiller-University, Jena, Germany.



Chris Lowery is a Research Associate at the University of Texas Institute for Geophysics. He is a foraminiferal micropaleontologist primarily interested in how ancient marine organisms responded to changes in their environment, and what that can tell us about modern ecosystem response to anthropogenic pressures. Chris received a BS from the University of Mary Washington, and a MS and PhD at the University of Massachusetts, Amherst. He was a shipboard biostratigrapher during IODP Expedition 364.



Christine Nims received her Bachelor's degree in Geology from the University of Colorado Boulder in 2016. She then worked as a research technician at Penn State University where she focused on the characterization of biomorphic carbon-sulfur microstructures using an array of analytical techniques including SEM, TEM, and Raman spectroscopy. She is currently a Master's student at the University of Michigan, studying microbial iron reduction and the formation of secondary biominerals in experimental systems simulating Precambrian iron sediments.



Bettina Schaefer received her Master's degree in Atmospheric Physics at the Goethe University Frankfurt (Germany). She is currently a PhD student at Curtin University working on the end-Cretaceous mass extinction event with Professor Kliti Grice. Her interests are in the organic geochemistry, in particular in

the biomarker profiles preserved in the Chicxulub impact crater IODP core.



Ellen Thomas received her Bachelor's, Master's and PhD degrees from the University of Utrecht (the Netherlands). She is a senior research associate at Yale University, and the Harold T. Stearns Professor of Integrative Sciences, the Smith Curator of Paleontology of the Joe Webb Peoples Museum of Natural History, and Research Professor in Earth and Environmental Sciences at Wesleyan University. She investigates the development of the highly diverse deep-sea faunas through periods of major climate change and mass extinction, focusing on assemblages and trace element and stable isotopic composition of benthic foraminifera (eukaryotic unicellular organisms).



Vivi Vajda is Professor and Department Chair at the Department of Paleobiology, Swedish Museum of Natural History in Stockholm, Sweden. Her research specialty is palynology, and her projects aim to determine the rate of turnover of plants across mass extinction events in Earth's history. Additional research includes chemical mapping of leaf fossils using vibrational microspectroscopic analyses. She is active in national and international geo-related organizations and was for several years chair of the Geological Society of Sweden and for the UNESCO sciences program IGCP. Since 2019 she is an elected member of the Royal Swedish Academy of Sciences and of the Hungarian Academy of Sciences.